The anatomy of a channel-fed ‘a‘ā lava flow system

Andrew Harris, S. K. Rowland, Oryaëlle Chevrel

The anatomy of a channel-fed ‘a‘ā lava flow system

A. J. L. Harris[1] · S. K. Rowland[2] · M. O. Chevrel[1]

Received: 22 September 2021 / Accepted: 1 June 2022

Abstract
The stabilized channel is a crucial element of an ‘a‘ā flow system, delivering lava to forward extending zones of dispersed flow. However, the term *stable* implies that channel geometries, lava properties, and dynamics are invariable. However, just how stable are these in space and time? To answer this question, we constrain the degree of variation for an extremely well-exposed stabilized channel on Kīlauea (Hawai'i), carrying out mapping, facies analyses, and sampling down the entire 5.5-km length of the channel-levee unit. Though active for only 3 days, flow and emplacement dynamics were highly unstable, experiencing both temporal and spatial variation. This resulted in a complex construction history and solidified channel form, where construction comprised three emplacement phases: initial, free-flowing, and late-stage ponded. These three emplacement phases were coupled with variation in underlying substrate, slope, and volume flux. These temporally and spatially varying conditions combined to result in four channel types and geometries (tubed, stable, ponded, and braided); five lava facies (smooth pāhoehoe, rough/spiney, slabby, transitional, and ‘a‘ā); and four levee types (initial-rubble, surge-fed overflow, pond-fed overflow, and accretionary). Complexity in channel form was reflected in cooling rates that ranged from 6.6 °C km^{-1} for free-flowing conditions to 17.7 °C km^{-1} for ponded lava. Likewise, vesicularities ranged from gas-rich (as high as 74% vesicles) to outgassed (as low as 27%). Due to the high degree of variance at this system, we suggest that *feeder channel* is a better term for this component of a channel-fed ‘a‘ā lava flow field. This term stresses the role of the channel in feeding zones of dispersed flow and is not a term that implies channel form and flow dynamics are unchanging. Although flow conditions can be complex, flow for some periods can be stable. If depths, widths, temperatures, and crystallinities during phases of below-bank stability can be identified, then the system can be modelled. We show this by fitting down-channel variation in flow properties for stable periods to output of the FLOWGO thermorheological model. In doing this, we provide a dataset that can guide and benchmark models aimed at simulating the dynamics and properties of channel-fed systems.

Keywords Lava channel · Levees · Vesicularity · Cooling rate · Crystallization rate · Mauna Ulu · Kilauea · Benchmark

Introduction

A lava channel unit comprises solid banks (the levees) between which lava flows (in the channel) and is one of two types of feeder system involved in lava flow emplacement, the other being tubes. Based on observations of Mauna Loa's 1984 channel-fed ‘a‘ā flow system, Lipman and Banks (1987) set up a four-fold classification to describe the down flow evolution of the system. This system comprised (i) a stabilized channel zone, (ii) a transitional channel zone, (iii) a zone of dispersed flow, and (iii) the flow toe. This down-flow organization of channel-fed ‘a‘ā system has since been identified as widely applicable, being found at many other basaltic effusive centers, including Etna (Favalli et al. 2010a), Piton de la Fournaise (Rhéty et al. 2017), and Mount Cameroon (Wantim et al. 2013), but also being applicable to basaltic-andesite (Castruccio and Conteras 2016), andesitic (Cigolini et al. 1984; Borgia et al. 1983) and dacitic (Harris et al. 2004) lava flow systems. Within such channel-fed systems defining the stable channel, and understanding the flow dynamics

Editorial responsibility: M.R. James; Deputy Executive Editor: L. Pioli

✉ A. J. L. Harris
andrew.harris@uca.fr

[1] Université Clermont Auvergne, CNRS, IRD, OPGC, Laboratoire Magmas et Volcans, 63000 Clermont-Ferrand, France

[2] Department of Earth Sciences, School of Ocean and Earth Science and Technology, University of Hawaii at Manoa, 1680 East-West Road, Honolulu, HI 96822, USA

associated with its evolution, is of particular importance since it typically accounts for more than half of the system by length (e.g., Mazzarini et al. 2005; Favalli et al. 2010a; Lipman and Banks 1987). It also delivers lava into the forward advancing portion of the system, and thereby determines the physical properties of lava arriving in the zone of dispersed flow as well as the volume flux feeding flow front advance. However, the "stable" label given to this component of the system implies invariance. By definition, the term *stable* evokes notions that a system is "firmly fixed" and thus not easily "changed or unbalanced or destroyed or altered" (Sykes 1982). Likewise, Merriam-Webster's (2014) define stable as "firmly established (fixed); not changing or fluctuating (unvarying or permanent)." As a result, the idea that steady-state flow within a channel of invariant geometry is generally triggered by the words "stable" and "channel." Stability is, in fact, often the simplifying assumption invoked when thinking of lava channels. However, the degree of variability of both channel and levee geometry, as well as flow dynamics, lava properties and lava type down this component of the system has rarely been assessed, and the benchmark for a stabilized channel remains that provided by Lipman and Banks (1987).

If we are to adequately understand and model the construction of a channel-fed ʻaʻā flow system or the associated flow thermorheological properties and dynamics (e.g., Glaze et al. 2009; Tallarico and Dragoni 1999; Harris and Rowland 2001; Kerr et al. 2006), the variability of stabilized channel morphology, flow properties, and dynamics must be fully defined and linked to the formative processes. Such ground truth is also essential support for interpretations regarding emplacement conditions based on geological observations of ancient (e.g., Passey and Bell 2007; Li and Liu 2020; Marin et al. 2020) and planetary (cf. Garry et al. 2007) systems, the emplacement of which was unobserved or outcrop is poorly exposed. To provide this ground truth, we present the results of detailed mapping and sampling of a 5.5-km-long channel that was active during the 1969–1974 Mauna Ulu eruption of Kīlauea (Hawai'i). We use the resulting map, channel profiles, and facies analysis, along with sample textural and glass chemistry properties, to describe the spatial and temporal complexity of a stabilized channel zone. Due to its excellent exposure, and pristine, unburied and (relatively) simple form, as well as the abundance of glassy samples down a length of more than 5 km, we identify this channel as being well suited for benchmarking of thermorheological- and physics-based models applied to channel-fed ʻaʻā flow systems (e.g., Miyamoto and Sasaki 1997; Hidaka et al. 2005; Vicari et al. 2007). We thus provide our data as a series of online resource items to serve as a benchmark for lava flow modelling. We use the data to test the FLOWGO model of Harris and Rowland (2001), which also allows us to apply caveats as to how the benchmark should be applied.

The stabilized channel: the state of knowledge

The channel-fed ʻaʻā flow system defined by Lipman and Banks (1987) involved, proximally-to-distally, the following four components:

(i) a stabilized channel zone across which all "marginal deformation of the flow ceased, (and) all movement became concentrated in the central channel, producing a stable geometry."
(ii) a transitional channel zone comprising "a distinct channel containing incandescent clinker ʻaʻā, bounded by blocky or clinkery lava a few tens of meters wide still capable of deforming or moving slowly."
(iii) a zone of dispersed flow where "movement is dispersed across much of the flow width and a central channel is poorly developed or absent."
(iv) the flow toe, which is the actively advancing flow front.

This system will lengthen with time as lava flowing through the stabilized zone is delivered to the advancing flow toe, with the dispersed and transitional channel zones developing behind the extending flow front (Lipman and Banks 1987). Following Guest et al. (1987) system spatial extension will be complete when the cooling-limited length is attained, but the four-zone organization will remain whether the flow is cooling or volume limited (Soldati et al. 2018). However, although the system will increase in complexity with time, gaining more and more branches or units (Kilburn and Lopes 1988, 1991), the basic down-system organization of each unit will retain these four component parts (e.g., Cigolini 1984; Wantim et al. 2013; Rhéty et al. 2017).

Cooling and crystallization conditions down the stabilized channel will determine the thermal and rheological conditions of lava delivered into evolving transitional channel and dispersed flow zones, as well as into the advancing, or stalling, flow toe (e.g., Harris and Rowland 2001; Rhéty et al. 2017; Soldati et al. 2018). The related down-system evolving fluid dynamic and rheological conditions (shear stress, strain rate, viscosity and yield strength) determine the morphological evolution of the lava moving through the stabilized channel (e.g., Soule et al. 2004; Riker et al. 2009; Sehlke et al. 2014). Measurements of cooling rates through stabilized channels indicate repeatable cooling trends, with

a range of 4 to 7 °C km^{-1} (Crisp et al. 1994; Cashman et al. 1999; Soule et al. 2004; Riker et al. 2009; Robert et al. 2014; Rhéty et al. 2017; Chevrel et al. 2019). Likewise, assessments of pāhoehoe–'a 'ā transitions (e.g., Peterson and Tilling, 1980; Kilburn 1981; Sehlke et al. 2014) and evolution of 'a'ā surface forms (Kilburn and Guest 1993) assume a systematic and non-reversible down-system evolution.

However, stability is not the case for all channel components. Levee forms, for example, show variety in space and time (e.g., Sparks et al. 1976; Lipman and Banks 1987; Naranjo et al. 1992). Stable channel formation involves emplacement of *initial levees* (Sparks et al. 1976) as broad lateral zones of the initial flow stall and stagnate either side of the central, flowing, zone (Hulme 1974; Lipman and Banks 1987), as well as *rubble levees* caused by avalanching of breccia from the advancing flow front and sides (Sparks et al. 1976). Subsequent changes in flow level associated with variations in supply can then emplace *overflow levees* on top of the initial levees if the increase in supply overwhelms the channel capacity (Bailey et al. 2006). Instead, if a rise or fall in level remains within the channel *accretionary levees* will be plastered to the channel walls (Walker 1967; Naranjo et al. 1992), and/or a prolonged phase of below-bank flow can result in *nested levees* (Lipman and Banks 1987; Harris et al. 2009).

The variety of levee type down a stabilized channel also implies that the flow dynamics associated with construction of each levee unit changed in time, i.e., at any single point along the channel, and/or space, i.e., with distance down the channel (e.g., Naranjo et al. 1992; Harris et al. 2009; Applegarth et al. 2010; Suh et al. 2011; Rhéty et al. 2017). The associated flow dynamics can thus also be highly variable over short temporal and spatial scales. Surges in supply can feed overflow, changes in flow level and flow velocity can wax and wane over periods of minutes (e.g., Bailey et al. 2006; James et al. 2007, 2010; Favalli et al. 2010b). These short-term variations can be superimposed on structures and dimensional properties resulting from longer-term (days-to-weeks) declines in flow rate (Naranjo et al. 1992), where progressive decreases in lava flux can build a series of nested levees (Applegarth et al. 2010). Levee type can also change down the system over distances of a few meters around zones of levee failure and their associated breakout flows or around blockages and their associated pond-fed overflow (e.g., Lipman and Banks 1987; Harris et al. 2009; Applegarth et al. 2010).

Other complications and complexities result from degassing and/or outgassing during down-channel lava flow or storage in syn-channel ponds to alter the rheology of the lava (cf. Sparks and Pinkerton 1978; Harris et al. 2020). Outgassing will alter the vesicularity and morphology of the lava, generating denser pāhoehoe forms, such as blue glassy, spiney, toothpaste or transitional, in place of low density spongey pāhoehoe and sheet flow forms (Swanson 1973; Rowland and Walker 1987; Wilmoth and Walker 1993; Sage 2000; Harris et al. 2017).

Changing rheological conditions due to changes in velocity and shearing will also push the lava through the pāhoehoe–'a 'ā transition. Although any packet of lava can never change from 'a'ā back to pāhoehoe, the interior of an 'a'ā flow can breakout to feed pāhoehoe (Jurado-Chichay and Rowland 1995), and at any one place in a channel lava passing that point can change from 'a'ā to pāhoehoe through time (Hon et al. 2003). In addition:

- late-stage flow or reduced velocities in distal or ponded sections cause increases in cooling rates per unit distance (Rhéty et al. 2017; Chevrel et al. 2019),
- stable channels can braid on steep slopes (Dietterich and Cashman 2014),
- anabranches and tributaries form due to levée failure (Applegarth et al. 2010), and
- blockage-and-pond systems may develop and decay (Lipman and Banks 1987; Bailey et al. 2006; Harris et al. 2009).

A stabilized channel is therefore by no means to be expected. Thus, we here use Mauna Ulu's Muliwai a Pele channel-fed 'a'ā flow system (Fig. 1a) to assess and quantify the degree of temporal and spatial variance in and down a stabilized channel. We use this assessment to consider whether the degree of variance in flow dynamics, geometry and lava properties merits the term *stable*.

Geological setting and context

Kīlauea's 1969–1974 eruption began on May 24, 1969 from a 4-km-long set of fissures that opened on the upper East Rift Zone between Alae and 'Ālo'i pit craters (Swanson et al. 1979). The eruption site became focused at a primary vent named Mauna Ulu (Fig. 1a). The eruption continued for 5 years and 2 months (901 days), ending on July 22, 1974, but experiencing a pause between October 15, 1971, and February 3, 1972 (Tilling et al. 1987). During this time, a 121-m-high parasitic shield developed at Mauna Ulu (Swanson et al. 1979; Tilling et al. 1987) hosting a lava lake (Duffield 1972; Tilling 1987) and 12 fountaining episodes (Parchetta et al. 2012). This activity fed channel- and tube-fed 'a'ā and pāhoehoe that extended 12 km to the coast building a 61 km^2 lava flow field (Holcomb 1976). While Swanson (1973) used observations of lava flow emplacement during the Mauna Ulu eruption to describe and classify types of pāhoehoe, Peterson et al. (1994) used the eruption to review modes of lava tube formation. In addition, Moore et al. (1973) used observations of lava flowing underwater at and off-shore of ocean entries to define pillow lava

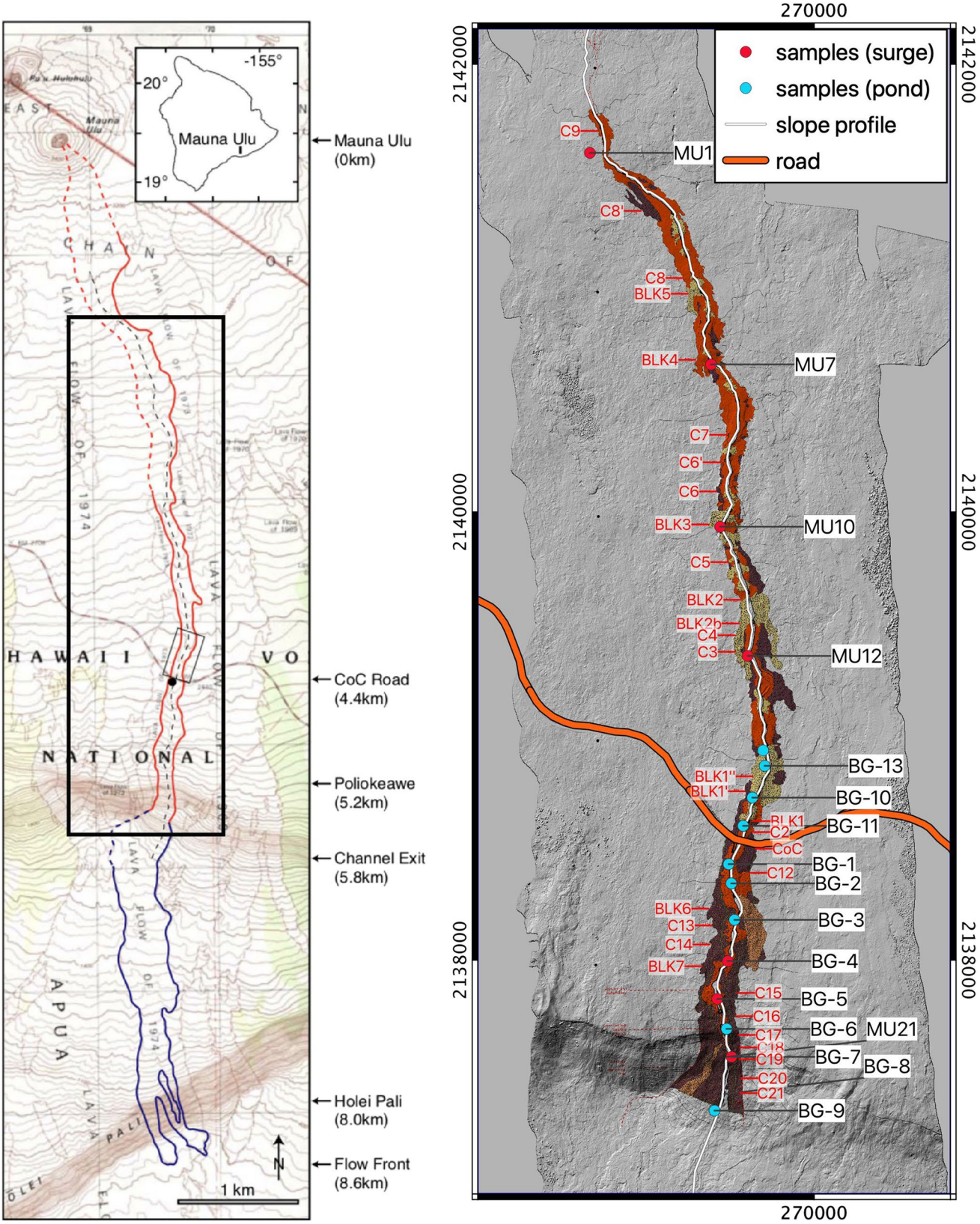
-155°
20°
19°
Mauna Ulu
Mauna Ulu
(0km)
CHAIN OF
FLOW OF 1974
LAVA FLOW OF 1973
HAWAII VO
NATIONAL
CoC Road
(4.4km)
Poliokeawe
(5.2km)
Channel Exit
(5.8km)
APUA
LAVA FLOW OF 1974
PALI
Holei Pali
(8.0km)
N
Flow Front
(8.6km)
1 km
270000
2142000
2140000
2138000
samples (surge)
samples (pond)
slope profile
road
C9
MU1
C8'
C8
BLK5
BLK4
MU7
C7
C6'
C6
BLK3
MU10
C5
BLK2
BLK2b
C4
C3
MU12
BG-13
BLK1''
BLK1'
BG-10
BLK1
C2
BG-11
CoC
C12
BG-1
BG-2
BLK6
C13
BG-3
C14
BLK7
BG-4
C15
BG-5
C16
C17
BG-6
MU21
C18
C19
BG-7
BG-8
C20
C21
BG-9

◂**Fig. 1** **a** Location map for the Muliwai a Pele channel modified from Harris et al. (2009). The abbreviation "COC" is for the Chain of Craters road, red outline gives the section characterized by the stable channel (as mostly considered here), and blue outlines the zone of transitional channel and dispersed flow. The thin black outlined box gives the zone considered by Harris et al. (2009), and the thick black outlined box gives the zone considered here, as given in **b**; black dot locates the Muliwai a Pele channel tourist overlook as signposted from the COC road pull off that cuts the right bank levee of the unit. **b** Geological map of the channel unit (as given in full in Online Resource 1) with main sampling locations for texture and petrology. Units are color coded as follows: Brown = ʻaʻā basal unit; yellow = blockage-fed overflow; orange = surge-fed overflow; salmon = secondary ʻaʻā due to late-stage breakout from main channel. See Online Resource 1 for full legend and detail of map sheet

emplacement dynamics. However, no use of the event was made to describe channel-fed ʻaʻā units.

Mapped as a channel-fed ʻaʻā unit by Holcomb (1980), the Muliwai a Pele lava channel system was formed during a short, final episode of fountain-fed activity that began late in the evening of May 29, 1974 (Tilling et al. 1987, p. 441–442; Carr and Greeley 1980, pp. 153–170). The channel system takes its name, which means Pele's River (Pukui and Elbert 1986), from the Hawaii Volcanoes National Park (HVNP) roadside stop on the Chain of Craters Road (Hazlett 1993). This road, and puff-off (Fig. 1a), was built after the eruption and at the time the eruptive episode had no name, being referred to by date in the Hawaiian Volcano Observatory (HVO) monthly report. The HVO monthly report described the episode as follows (HVO 1974):

> Quite abruptly, late on the evening of 29 May, Kilauea's summit began to deflate steadily, and tremor at Mauna Ulu increased. On the morning of the 30th, a trip to Mauna Ulu's summit revealed that the summit crater had refilled to the brim, and was spilling over at two places on the southeast rim. A flow had travelled almost 2 km to the south […] fountains and overflows continued throughout 31 May.

By the following morning HVO (1974) reported:

> The morning of 1 June dawned crisp and clear and, fortuitously, aerial photographers were on the Big Island, and chose this morning to fly the bad-weather-plagued and now overdue photo reconnaissance of the Mauna Ulu area. The resultant photographs (three flight lines) were flown at the very peak of the eruptive activity on a cloudless (except for fume) day. These photos show the active vent at Mauna Ulu with the summit appearing as a bright flower with 'petals' of lava pouring down all sides of the shield in deep, brim-full channels. Most of the lava travelled to the south, and these remarkable photos follow the active flow nearly 9 km to the south and show lava pouring over both Poliokeawe and Holei Palis. The lower part of the flow is aa, and the photos provide clear views of the pahoehoe-aa transition. (original text and punctuation retained)

The overflow that fed the channel system stopped around 02h00 (Hawaiian Standard Time) on June 2 having lasted around 50 h, with the May 29–June 2 eruptive episode adding 4 m of lava to the Mauna Ulu shield (Tilling et al. 1987).

Unfortunately, the remoteness of the site made channel formation and flow dynamics impossible to observe. However, a photo published in Greeley (1974), Tilling et al. (1987) and Carr and Greeley (1980) shows the channel between (what is today) the Chain of Craters road and the base of the Poliokeawe Pali (Fig. 2a). From this, we see a single channel of variable width above Poliokeawe Pali. On the steep slopes of the Pali, the channel system is braided and recombines below the Pali into single, but broad, channel (Greeley 1974). Three photographs of the distal portion of the channel and the flow front were also taken from an aircraft on 1 June 1974 and are available as photographic slides in the HVO archive, as is one slide of the vent area. An additional slide is available, taken on 20 June 1974, looking across the lava lake in the Mauna Ulu pit and towards the point of exit for the flow (Fig. 2).

The excellent exposure of this well-developed channel has meant that it has become a target for visitor guides (Hazlett 1993; Hazlett and Hyndman 1996) and studies aimed at mapping lava types associated with channel-fed emplacement (Harris et al. 2009; Robert et al. 2014; Whelley et al. 2017). We began mapping and sampling the channel system in March 2002, and completed an additional seven field campaigns between 2002 and 2012.

We have so far used these data to support three papers published in series (Harris et al. 2009; Robert et al. 2014; Sehlke et al. 2014). In the first, we described levee and channel structures down a 200-m length of the system to examine channel construction processes and the flow dynamics responsible for the channel–levee structures (Harris et al. 2009). We also defined the channel as forming in a three-stage process whereby (Harris et al. 2009):

1. The channel became established roughly central to the stalled margins (initial and rubble levees) of an ʻaʻā flow that we estimated was erupted at 35 m^3/s.
2. Thereafter, short-lived (≤ 5 min-long) pulses of lava down the channel at 90–420 m^3/s fed overflows of pāhoehoe to build a levee-capping unit. During surges, blocks were plucked from the channel wall to be floated down channel to contribute to blockages. At the end of the episode, lava became ponded behind the blockages to form a series of syn-channel ponds.

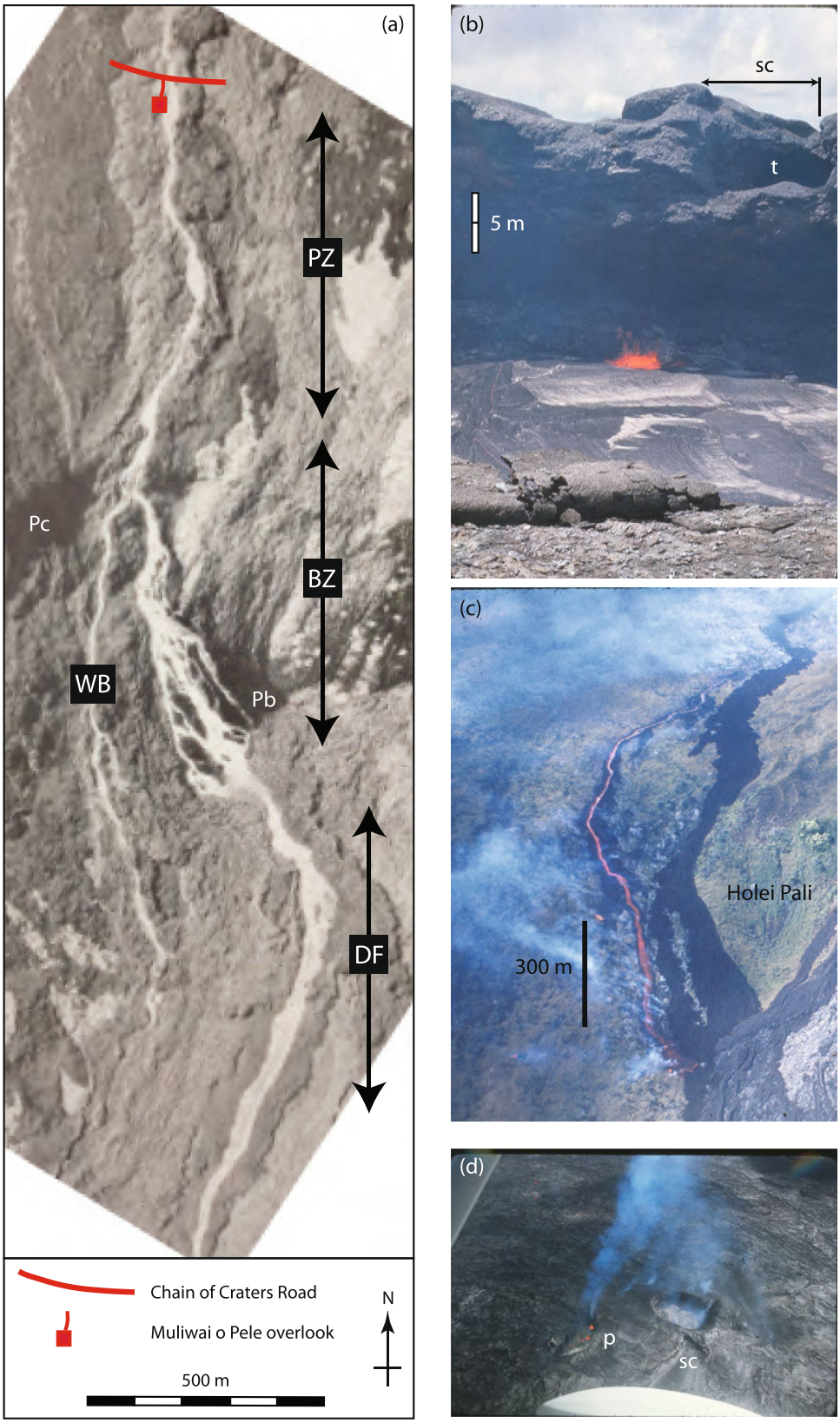

Fig. 2 **a** Aerial photo of the Muliwai a Pele channel as active and descending the Poliokeawe Pali on the morning of 1 June 1974 (HVO 1974). The photo was acquired by the R.M. Towill Corporation (Greeley 1974; Tilling et al. 1987) and is here scanned from Greeley (1974, p. 71) as the originals from this overflight have been lost. The photo has been rotated so that North is up and mirrored so that West is left. The current location of the Chain of Craters road and Mulawai o Pele overlook have been approximately placed. PZ = ponded channel zone; BZ = braided channel zone; DF = dispersed flow; WB = secondary channel (west branch of the braided system); Pc = Poliokeawe Pali crest; Pb = Poliokeawe Pali base. **b** photograph looking south across the Mauna Ulu lava lake on 20 June 1974 into the tube (t) and spillway channel (sc) that fed the Muliwai a Pele channel system. Lava lake surface is around 20 m below the pit rim (photograph source: USGS-HVO Mauna Ulu Slide Book 28, p. 12, Photograph 25; Photograph Credit: D.W. Peterson). **c** Photograph looking north across the actively advancing flow front and up the distal section of the system on 1 June 1974. Scale bar is for the foreground on Holei Pali (photograph source: USGS-HVO Mauna Ulu photograph Book 28, p. 9, Photograph 4; Photograph Credit: D.W. Peterson). **d** Photograph looking down onto the Mauna Ulu lava lake and Mulawai o Pele spillway channel sometime on 1 June 1974. Channel already appears to be roofed over, and pāhoehoe (p) is already advancing over it on its eastern edge from a small lateral vent on the flank of the Mauna Ulu shield (photograph source: USGS-HVO Mauna Ulu Photograph Book 28, p. 9, Photograph 37; Photograph Credit: D.W. Peterson)

3. In a final phase of channel construction that lasted a further ~10 h, the roofed-over ponds continued to drain through the blockages to cause roofs to founder, and inflated flows to be emplaced on the channel floor below each blockage.

We have also carried out textural and chemical analyses of samples collected down the channel length to build a rheological model for the lava, as well as to define down-flow textural and cooling trends (Robert et al. 2014). In Sehlke et al. (2014), we linked these with flow rheology and the pāhoehoe-'a ʻā transition. Although the cooling rate down the channel was estimated to have been constant at 6.7 °C/km, the crystallization rate increased from 0.03Φc/km in the proximal zone to 0.14Φc/km in the distal zone (with Φc being the crystal fraction). This controlled lava viscosity and yield strength increase that were estimated to have an average of 150 Pa s and 140 Pa, respectively, in the proximal zone, and 2000 Pa s and 400 Pa, respectively, in the distal zone (Robert et al. 2014). Sehlke et al. (2014) experimentally measured the viscosity of remelted samples and showed that the transition from pāhoehoe to ʻa‘ā surface textures begins at a crystallinity of ~10% and ends at crystal contents exceeding 40%. The pāhoehoe to ʻa‘ā transition begins to occur at the same spatial (Robert et al. 2014) and rheological (Sehlke et al. 2014) point in the channel after a distance of 4.5 km and a viscosity of 250 Pa s.

Here, in this fourth paper of the series, we present the full description of the Muliwai a Pele lava channel system. This includes:

- the geological map for the stabilized channel (Online Resource 1; Fig. 1b),
- a detailed description of all morphological features, and
- new data from a sampling campaign made in 2017 that was prompted by gaps in the data set revealed by the analysis of Robert et al. (2014).

We use this to:

(i) define and classify the down-system channel and levee morphology,
(ii) link the down-system changing morphologies to the formative emplacement processes,
(iii) properly explain the associated down-flow cooling and crystallization trends, and
(iv) provide and test a benchmark for lava flow modelling.

We provide all data in Online Resources 2 through 5, and the benchmark in Online Resources 6–9.

Methods

We mapped the Muliwai a Pele channel and lava flow using a 0.82-m-spatial-resolution panchromatic IKONOS image (https://www.satimagingcorp.com/satellite-sensors/ikonos/) and the US Geological Survey (USGS) 7.5-min map sheet of Makaopuhi Crater (U.S. Geological Survey 2017). This map sheet also served as a contour underlay for the geological map (Fig. 1; Online Resource 1). Note that we follow fluvial flow terminology and define right and left with respect to the channel when looking in the down-flow direction. In our case, flow was to the south so that the right bank is to the west, and left bank is to the east. We also define a levee as being a part of the channel system built during a single, discrete deposition event, such as short-lived overflow from of the channel, with the bank being the static margin of the channel built by successive levee forming events (cf. Whittow 1984). The bank can thus have a composite form involving multiple levees. In the field, we walked all unit perimeters and channel rims with a hand-held GPS, as well as the right- and left-bank channel rims. The precision of the GPS-walked lines was that given by the sensor (a Garmin Etrex) and was typically 1–2 m. This is roughly the same as the precision of the mapping using IKONOS, i.e., one to two 1 m pixels. Overlaying GPS-walked lines with IKONOS-mapped contacts revealed agreement within the ± 1 m limit precision of the two data sets.

In addition, changes in grayscale tone in the IKONOS image were used to map the lava surfaces down the channel system, as well as the channel left and right bank margins. Fieldwork allowed us to link all tone changes to lava surface types, which we placed into five facies following the classification system of Harris et al. (2017). These were linked to their grayscale appearance in the IKONOS imagery following the look-up table of the Color Wheel Company (Arts Cool Graphics Group 2006) which provides a light reflectance value scale between 0% (i.e., black or zero on an 8-bit gray scale) and 100% (i.e., white or 255 on an 8-bit scale):

(i) ʻa‘ā: black (< 20%);
(ii) slabby pāhoehoe: dark tones (20–40%);
(iii) transitional pāhoehoe: dark-to-moderate tones (40–60%);
(iv) spiney (rough-surfaced) pāhoehoe: moderate-to-light tones (60–80%); and
(v) smooth pāhoehoe: light tones (> 80%).

All changes and associations were checked and confirmed in the field, revealing an uncertainty in the lava type contacts of ± 1 m. Following Sparks et al. (1976) and Lipman and Banks (1987), we placed levee unit types into three classes:

(i) initial and rubble levees (the basal unit);
(ii) overflow levees emplaced during surges that overwhelmed the channel capacity to emplace a short-lived overbank emplacement event (surge overflow units); and
(iii) overflow levees emplaced during backup behind blockages (blockage overflow).

All channel blockages were GPS-located and flows breaking out of the channel classified into flow fed by:

(i) failure of a channel wall, and
(ii) flow fed by prolonged overflow (during either a surge or ponding behind a blockage).

Finally, we mapped all underlying contacts between lava flow units emplaced earlier in the Mauna Ulu eruption using the date-tagged unit maps of Holcomb (1976, 1980) and the US Geological Survey (2017). As part of this, detailed (0.25 m resolution) maps of four case type locations were prepared for the proximal, upper medial, lower medial and distal sections of the channel, as given in Figs. 3 and 4. We present the resulting geological map as a full map sheet in Online Resource 1.

We defined channel morphologies at 21 locations (Table 1) termed "channel stations," following Lipman and Banks (1987) and Moore (1987). Channel stations were selected as being representative of any particular channel form and dimension down any given reach. At each channel station, we defined the type and number of levee units, as well as the character of the lava making up the in-channel or outer levee units. For each station, measurements were also made to derive all channel and levee dimensional parameters (Fig. 5) using tape measure, compass-clinometer and laser range finder. Heights, thicknesses, and depths measured using the laser range finder have an uncertainty of 0.01 m, and those with the tape measure (as checked through repeat measurements) are 0.1 m. This, coupled with the natural variation of the feature which is not perfectly planar, we round all vertical dimensions to 0.1 m and the uncertainty on all given values is ± 0.05 m. Instead, uncertainty for distances greater than 10 m is 0.5 m, so such values are rounded to the nearest meter and have an uncertainty of 0.05 m. In the same way, the uncertainty on all angle measurements was found to be 1° or ± 0.5°. Around stations C8, C5, C4, CoC, C14-16 and C19-20 (Fig. 1) we made the dimensional measurements of Fig. 5 every 10 to 30 m for a distance of 60–300 m

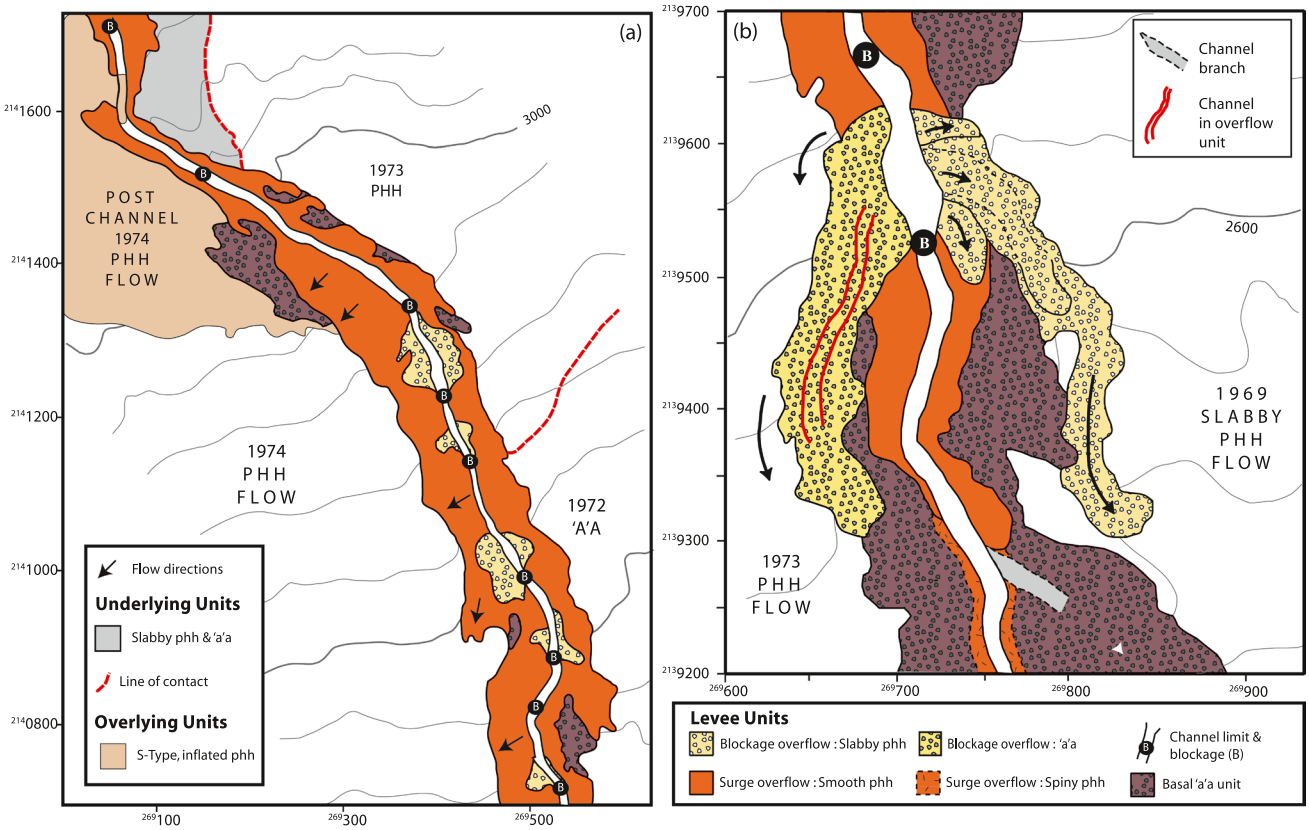

Fig. 3 Maps of the upper-medial reach of the channel system between stations **a** C9 and BLK 4–5, and **b** BLK2 and C3-BLK1' (see Fig. 1 for locations)

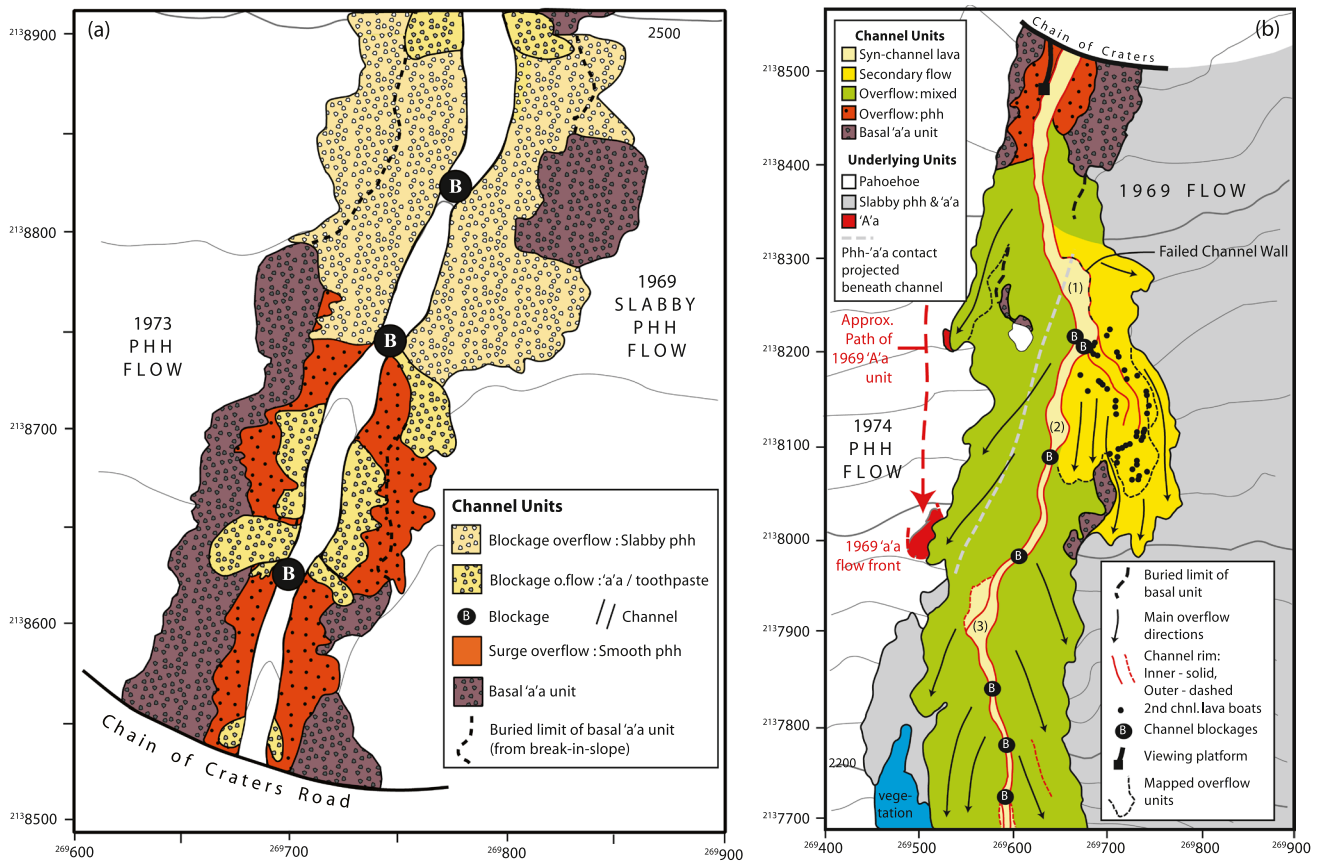

Fig. 4 Maps of the medial-distal reach of the channel system between stations **a** BLK1' and COC, and **b** COC and C17, where three broad ponded lengths are marked (1), (2), and (3) (see Fig. 1 for locations)

up-flow and/or down-flow from the station. These measurements were used to confirm the representivity of each channel station in terms of describing the channel morphology and dimension for any given reach. We provide the full dataset of measured and derived channel dimension values in Online Resource 2, and the cross-channel profiles and all geological sections are given in Fig. 6 (as also inset in the map sheet of Online Resource 1).

To allow generation of a statistically robust data set spanning the entire channel length, at all locations where overflow levees were apparent, we also measured the number and thickness of the overflow levee (h_L, in m) plus the underlying levee slope (α_L, in degrees), and collected a sample for density (ρ, in kg/m^3) (as given in Online Resource 3). This involved measurements at 98 locations (including at and around each channel station). Overflow levees could be defined by the surface expression of their flow front or from their exposure in cracks: see Fig. 7 of Harris et al. (2009) in which this is defined. Following Hulme (1974), the density measurement allowed yield strength (τ_0) to be estimated from $\tau_0 = h_L\ \rho\ g\ \sin(\alpha_L)$, g being gravity. In total we carried out measurements at 152 overflow units (as given in Online Resource 4).

In Robert et al. (2014), we presented a set of 28 of these samples as acquired in 2012 (Fig. 1; Supplement 3). On these we completed bulk chemistry, density, vesicle content and size distribution, plus glass chemistry and microlite crystallization analyses on the quenched (glassy) crust, and used the data to estimate lava temperature, cooling and crystallization rate. However, that dataset lacked samples between 4 and 6 km, a channel reach which marked an increase in cooling and crystallization (Robert et al. 2014). Thus, in 2017, we resampled this reach, as well as the flow front, identifying all possible glassy samples (Fig. 1). Note that most of the 152 samples collected for density measurements could not be used because of insufficient glass. On these new glassy samples, we used the same methodology as Robert et al. (2014) to derive glass chemistry and microlite crystallization, and hence temperature and crystallization rates. For glass chemistry, we used an electron microprobe (CAMECA SX 100: operating at 15 kV and with a 15-nA beam current) at the Laboratoire of Magmas et Volcans (Université Clermont Auvergne, Aubière, France). The spot size was 10 µm, and measurements were made where the glass was homogeneous and as far as possible from phenocrysts and microlites. Following Cashman et al. (1999)

Table 1 Locations of channel stations used to define flow profiles for channel morphologies. GPS format is North American Datum of 1983 (NAD83), "phh" is pahoehoe, and "distance" is distance from vent as defined by the vent rim marker (Fig. 1)

Profile	GPS (E)	GPS (N)	Distance (m)	Slope (°)	Lava structure/type	Channel form
RIM	268,776	2,142,863	0	12.7	Unconformity	Pit outlet
C11	268,818	2,142,724	160	9.2	Skylight	Tube
SKY4	268,860	2,142,622	260	9.2	Skylight	Tube
SKY3	268,891	2,142,573	320	9.2	Skylight	Tube
SKY2	268,876	2,142,418	470	9.2	Skylight	Tube
SKY1	268,861	2,142,367	525	9.2	Skylight	Tube
C10	268,859	2,142,330	700	2.6	Depression	Buried
C9	269,027	2,141,763	1240	3.5	Depression	Buried
C8B	269,182	2,141,496	1540	2.8	Smooth phh	Mature
C8	269,389	2,141,287	1930	3.5	Smooth phh	Mature
BLK5	269,394	2,141,262	2030	3.7	Smooth phh	Mature
BLK4	269,553	2,140,665	2580	3.9	Smooth phh	Mature
C7	269,654	2,140,396	2618	3.3	Smooth phh	Mature
C6	269,611	2,140,222	2818	2.8	Smooth phh	Mature
BLK3	269,590	2,139,971	3078	2.9	Smooth phh	Mature
C5	269,652	2,139,773	3268	3.1	Smooth phh	Mature
BLK2	269,691	2,139,652	3428	3.7	Smooth phh	Mature
C4	269,702	2,139,430	3618	3.1	Smooth phh	Mature
C3	269,697	2,139,369	3758	3.3	Smooth phh	Mature
C2	269,692	2,138,631	4258	3.5	Transitional phh	Mature
COC	269,656	2,138,522	4408	3.3	Transitional phh	Mature
COC	269,603	2,138,534	4408	3.3	Basal ʻaʻā unit	Initial levee
C12	269,626	2,138,389	4528	4.4	Transitional phh	Mature
BLK6	269,672	2,138,233	4648	7.0	Transitional phh	Ponded
C13	269,651	2,138,174	4728	6.3	Transitional phh	Ponded
C14	269,626	2,138,051	4828	6.2	Transitional phh	Ponded
BLK7	269,601	2,137,985	4918	5.2	Transitional phh	Ponded
C15	269,561	2,137,885	5018	7.0	Transitional phh	Ponded
C16	269,576	2,137,835	5118	20.1	Transitional phh	Ponded
C17	269,592	2,137,713	5218	17.0	Transitional phh	Ponded
C18	269,603	2,137,626	5308	18.5	ʻaʻā	Braided
C19	269,605	2,137,553	5408	15.3	ʻaʻā	Braided
C20	269,589	2,137,473	5508	15.3	ʻaʻā	Braided
C21	269,559	2,137,363	5608	15.3	ʻaʻā	Braided
FF	269,826	2,134,775	9000	3.3	ʻaʻā	Flow front

all compositions are given as averages of eight analyses. The counting time of 10 s was increased to 60 s for Mg, reducing analytical errors on MgO to 0.08–0.10 wt% (2σ). The MgO content was then used to obtain lava temperature following the method of Helz and Thornber (1987). Uncertainty on temperature was based on the 2σ data for the eight analyses, and was 1–3 °C. Crystal content in the glassy area of the thin section at the contact with the surface was estimated using backscattered electron (BSE) images, as collected by scanning electron microscopy (SEM) at magnifications of × 25 and × 100. One or two images per sample were processed and converted into binary images via ImageJ, and only crystals greater in length than 6 um (three pixels) were considered. The percentage of crystals was corrected for vesicularity as quantified on the same image. Based on an analysis of 16 thin sections the 2σ uncertainty in crystallinity is 2%. Density was obtained using cut sample volumes of known masses using an Accupyc 1340 Helium Pycnometer. The dense rock density of 2900(± 10) kg/m^3 for this lava flow (Robert et al., 2014) was then used to derive the vesicularity of each sample. All results are given as averages of five measurements, where the 2σ error in density is between 1 and 7 kg/m^3. This translates to an uncertainty in density values of 2–14 kg/m^3, and thus ± 1% on vesicularity. A full description of the methodology applied here for chemical and textural analysis is given in Robert et al. (2014).

We give these new results in Online Resource 5 where we update the texture tables and supplements of Robert et al.

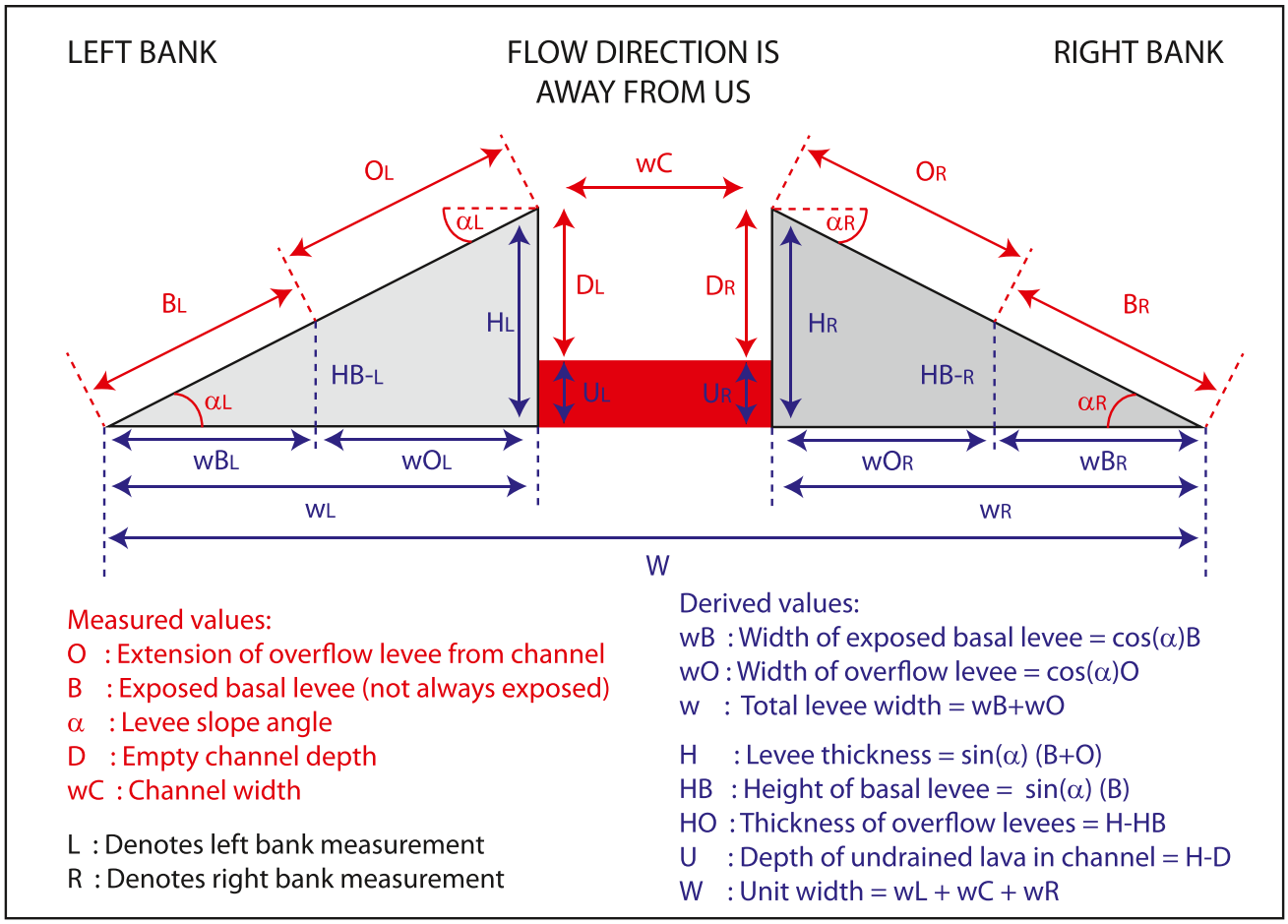

Fig. 5 Channel and levee geometry as measured and calculated as viewed looking in the down-flow direction as that flow direction is away from us

(2014). The complete dimensional, textural and temperature dataset for the entire Muliwai a Pele channel is thus given in the Online Resource. We also use these data to model the down-flow variation in lava thermo-rheological properties and velocity using FLOWGO (Harris and Rowland 2001). Initialization of the model, as well as the benchmark test, is given in Online Resource 6.

Results

The first 1.1 km of the channel is buried by later pāhoehoe overflows from Mauna Ulu (Fig. 2d). However, the line of the buried channel can be followed from the Mauna Ulu source to its first exposure from depression in the pāhoehoe through which the channel rim sometimes crops out and a line of eight skylights (see map of Online Resource 1). A U-shaped trough in the south wall of the Mauna Ulu pit crater, 16–18 m wide and 4–6 m deep, marks the channel exit. Beneath this there is a 12–14 m wide and 10–12 m deep unconformity (Fig. 7a), which matches the shape and dimensions of the outlet tube and channel photographed during the eruption (Fig. 2b). The first skylight (C11) is the largest and deepest, being 7.65 m across with a roof thickness of 3 m and an empty tube height of 1.7 m. The floor of the skylight is filled with rubble of unknown depth (Fig. 7b). However, the photograph of the active tube indicates around 3 m of head space and 2.5 m of undrained lava in the tube exiting the vent zone (Fig. 2b). The roof at C11 is composed of welded spatter either exposed or veneered with lava. Other skylights (SKY1–SKY4) are smaller and show a drained tube height of 0.8–2.4 m and a roof thickness of 0.6–1.45 m (Table 2). Tube form is unorthodox in that over a down-flow distance of 1–2 m a tube of ~ 50 cm in height and 2 m in width can narrow down to 50 cm in width and then open up again into a 3–4 m high-and-wide cavern. Caverns are drained down-flow by multiple outlet nozzles which narrow down from 50 cm at their exit from the cavern to less than 20–30 cm. Cavern walls are bulbous and veneered with glazed lava (Fig. 7c,d).

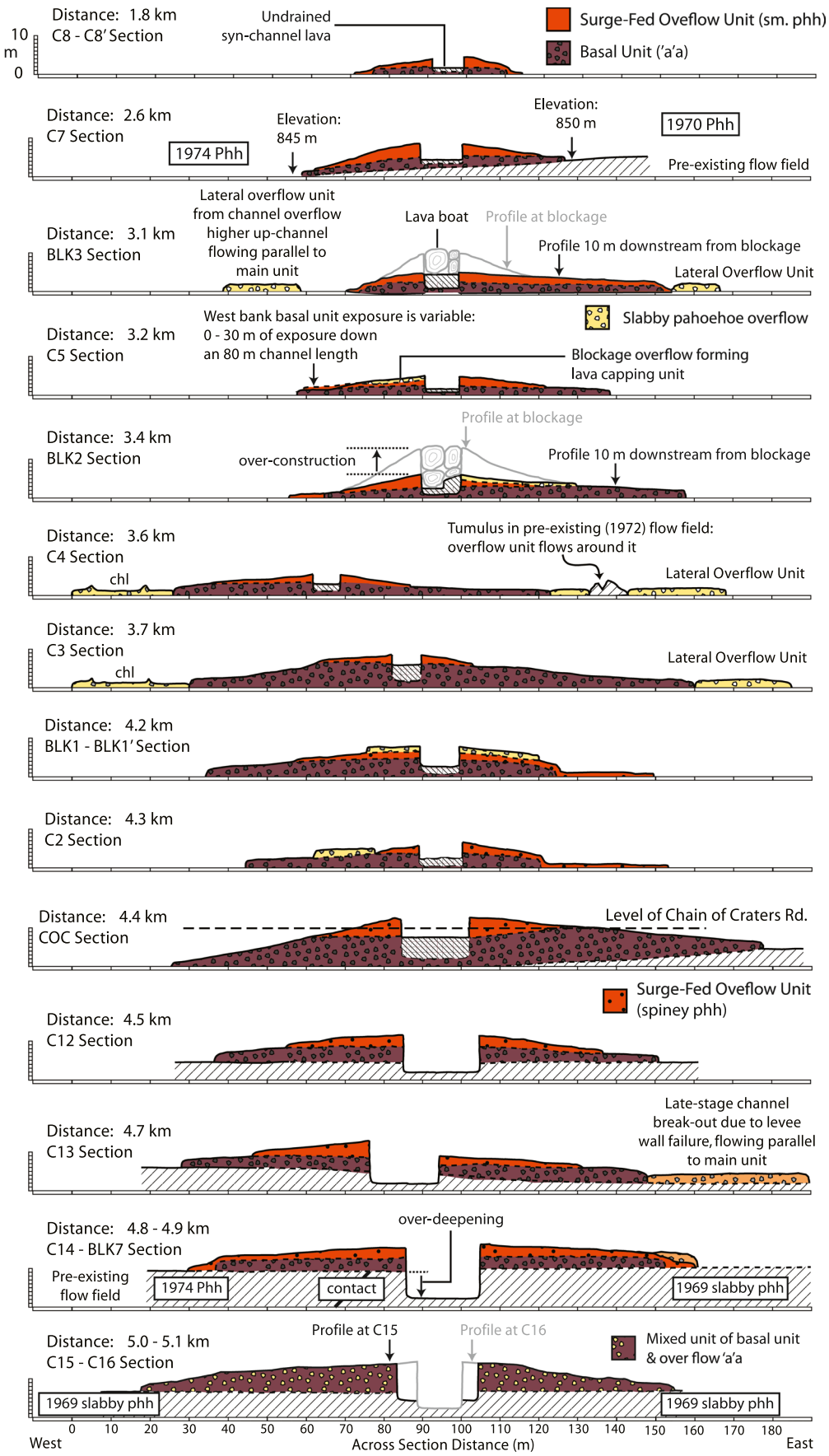
Distance: 1.8 km
C8 - C8′ Section
10
m
0
Undrained
syn-channel lava
Surge-Fed Oveflow Unit (sm. phh)
Basal Unit ('a'a)
Distance: 2.6 km
C7 Section
1974 Phh
Elevation:
845 m
Elevation:
850 m
1970 Phh
Pre-existing flow field
Distance: 3.1 km
BLK3 Section
Lateral overflow unit
from channel overflow
higher up-channel
flowing parallel to
main unit
Lava boat
Profile at blockage
Profile 10 m downstream from blockage
Lateral Overflow Unit
Distance: 3.2 km
C5 Section
West bank basal unit exposure is variable:
0 - 30 m of exposure down
an 80 m channel length
Slabby pahoehoe overflow
Blockage overflow forming
lava capping unit
Distance: 3.4 km
BLK2 Section
Profile at blockage
over-construction
Profile 10 m downstream from blockage
Distance: 3.6 km
C4 Section
chl
Tumulus in pre-existing (1972) flow field:
overflow unit flows around it
Lateral Overflow Unit
Distance: 3.7 km
C3 Section
chl
Lateral Overflow Unit
Distance: 4.2 km
BLK1 - BLK1′ Section
Distance: 4.3 km
C2 Section
Distance: 4.4 km
COC Section
Level of Chain of Craters Rd.
Surge-Fed Oveflow Unit
(spiney phh)
Distance: 4.5 km
C12 Section
Distance: 4.7 km
C13 Section
Late-stage channel
break-out due to levee
wall failure, flowing parallel
to main unit
Distance: 4.8 - 4.9 km
C14 - BLK7 Section
over-deepening
Pre-existing
flow field
1974 Phh
contact
1969 slabby phh
Distance: 5.0 - 5.1 km
C15 - C16 Section
Profile at C15
Profile at C16
Mixed unit of basal unit
& over flow 'a'a
1969 slabby phh
1969 slabby phh
0 10 20 30 40 50 60 70 80 90 100 110 120 130 140 150 160 170 180
West
Across Section Distance (m)
East

◂**Fig. 6** Cross-channel profiles and geological cross-sections for all stations for cases where the channel is fully exposed, i.e., between station C8 and the crest of Poliokeawe Pali, i.e., station C16 (see Fig. 1 for locations)

After the first point of exposure, the stable channel can be traced for 4.9 km to the base of Poliokeawe Pali (Fig. 1; Online Resource 1). Here the channel becomes poorly defined and transitional (senso Lipman and Banks 1987). Across the transitional channel zone, a broad central stream (in this case of order of 100 m wide) is bounded by incipient and simple initial levees. The central stream is approximately the same level as the banks, with the two being separated by a zone of shear (Fig. 8a). The transitional channel extends 2.4 km to the top of Hōlei Pali down which the flow lacks well-developed channel forms (Fig. 8b). Over Holei Pali the flow divides into two branches (Fig. 1), feeding two lobate ʻaʻā flow fronts, 170 m (W lobe) and 150 m (E lobe) across and 3–4 m high (Fig. 8c). The flow front is at the base of Hōlei Pali and the total channel-fed ʻaʻā flow system length is 9 km (Fig. 1). The stable channel section thus makes up 70% of the system by length and we herein focus on the morphology of its exposed length.

Lava boats, blockages, and syn-channel lava

Lava boats (senso Lipman and Banks 1987) are ubiquitous down both channel banks and consist of pāhoehoe-veneered chunks of levee (Fig. 9a). Where broken, the interior structure shows the boat to be comprised of stacks of thin overflow units plucked from the bank. Given the meter scale of the boats plucking must have involved bank areas within 1–3 m of the channel. The example of Fig. 9b shows the block to be of channel inner-bank and bank-proximal levee, which in this case is comprised of seven pāhoehoe overflow units. Lava boats are formed by bank failure where sections of levee become broken off and floated down channel (Lipman and Banks 1987). Boats can then be floated out of the channel during a phase of overbank flow to be deposited on the levee surface (Harris et al. 2009). Boats become coated in channel lava while rolling in the channel and/or plastered with lava during subsequent overbank flow events once emplaced (Fig. 9c). Lava boats are typically longer than they are wide and range in size from a few tens of centimeters to 7 m in long-axis length. They are typically found perched on the channel rim (Fig. 9c) and have been floated no farther than 10 m out of the channel.

There are 29 blockages down the channel (Fig. 1, Online Resource 1). Blockages comprise lava boats of 2–3 m across that have floated down-channel to become jammed in a constriction (Fig. 10a). Lava flowing over and around the resulting constriction causes over-construction of the channel at the blockage so that, in the case of the example of BLK2 (Fig. 10a), levees around blockages are up to four times higher than where lava had flowed freely within the channel. Blockages are porous so lava has also flowed through them (Fig. 10b). In the case of BLK3 large caverns exist within the blockage. Caverns contain internal lava falls and flow exits the caverns through a down-flow opening at the blockage base (Fig. 10b).

Lava arriving in the channel behind each blockage backed up to form stagnant lava ponds in the upstream channel (Harris et al. 2009). As a result, all in-channel lava behind blockages is associated with a stagnant pond. In some cases, ponds remained undrained so that the channel is brim full with ponded lava (Fig. 9c). In other cases, the fluid interior of the pond drained down-channel to leave the pond crust attached to the channel banks as a roof creating a tube-like structure (Fig. 11a). In most cases, removal of support during pond drainage caused the roof to subside or collapse, so that roof material is present as a jumble of slabs and blocks on the channel floor (Fig. 11b). In other cases, ponded lava inflated to generate tumuli with inflation clefts (Fig. 11c).

Down-flow lava draining through a blockage fed short flows of toothpaste lava (cf. Rowland and Walker 1987). The toothpaste lavas had their sources at the blockage base (Fig. 10a) and were up to ~ 19 m long (BLK2; Fig. 10a). Such lava units characterize the syn-channel lava form all the way to the crest of Poliokeawe Pali. Only on the steep (17–20°) slopes of Poliokeawe Pali do we find lava on the channel floor that was flowing freely in the channel when the supply ended and flow came to rest within the channel (Fig. 11d).

Levee lava facies

Down the channel, we identify the five main lava facies listed above (see also legend to map of Online Resource 1): smooth pāhoehoe, rough/spiney pāhoehoe, slabby pāhoehoe, transitional, and ʻaʻā (Fig. 12). Smooth pāhoehoe is characterized by a flat, glassy surface in which ropes and lobes are rare and lava is typically present as overbank sheet flow that mantles lava boats (Fig. 13a). Vesicularities have a range of 44–74% with a mean of 59 ± 6% (Table 3). The surface is highly reflective and golden in sunlight. Phenocrysts of olivine trapped in the glassy selvage cause small (mm-scale) bumps on the surface, and drawn out vesicles (with walls stretched in the flow direction) result in a fibrous surface fabric (Fig. 12c). Rough pāhoehoe is also associated with overbank sheet flow, but lacks the coherent glassy crust of smooth pāhoehoe (Fig. 12d). Surfaces have a low reflectance and are dull in sunlight. The end-member of rough pāhoehoe is spiney pāhoehoe, where walls of large (cm-scale) vesicles have been drawn out across the flow surface to break and form spines (Fig. 12e). Spiney pāhoehoe is generally associated with syn-channel, ponded lava overflowing from lava

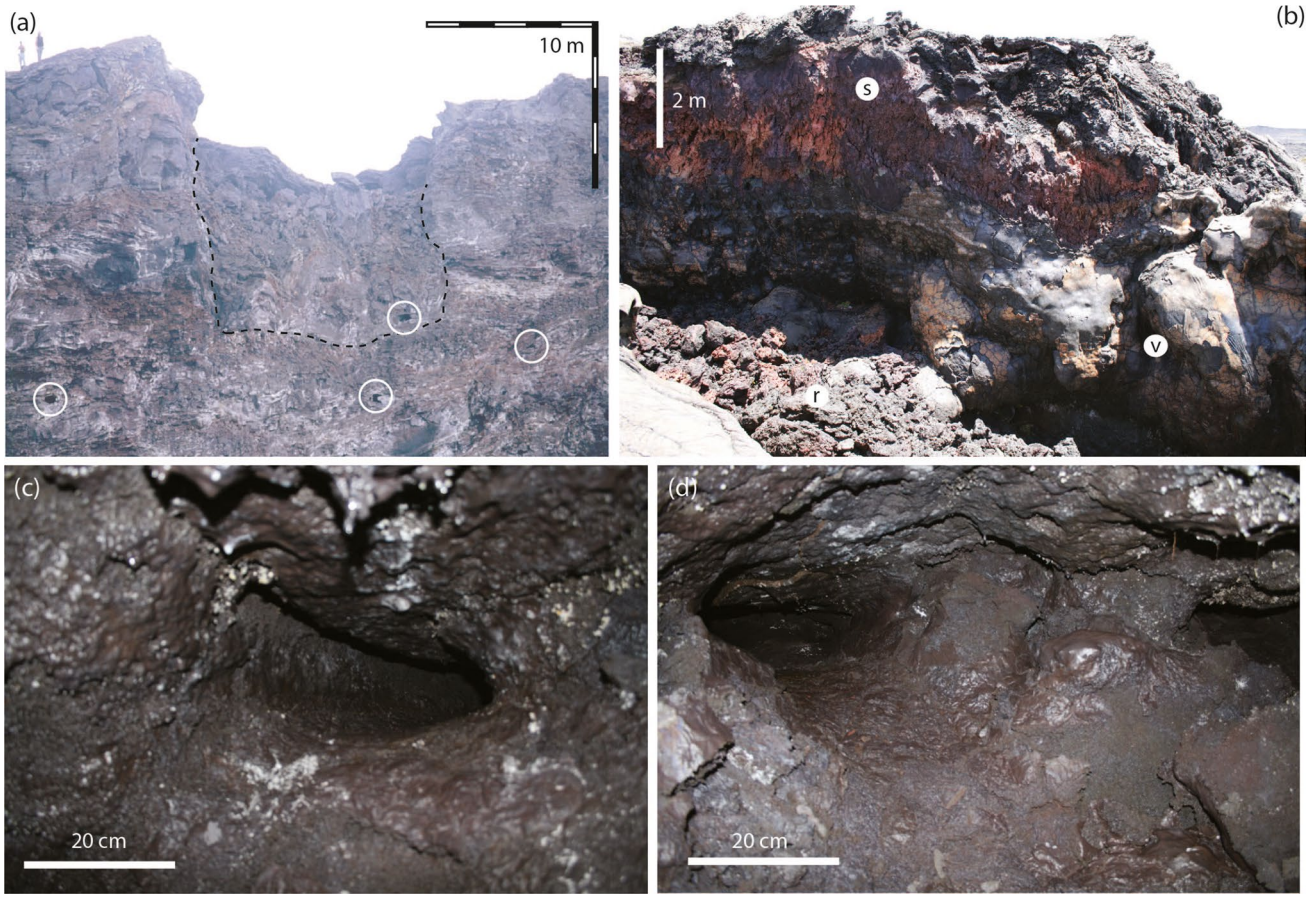

Fig. 7 Photos of the proximal (buried and tubed) section of the channel system. **a** View looking south across the Mauna Ulu pit to the unconformity (dashed black line) marking the outlet of the Muliwai a Pele channel (small tubes marked by white circles). This is a view from the same position and direction as in Fig. 2b. **b** View looking east across skylight C11 showing welded spatter (s) and lava-veneered spatter (v) in its east wall, and rubble (r) on the floor. **c** Left and **d** right bank outlet nozzles from the cavern at skylight SKY-3, showing smooth, shiny, metallic-gray, glaze typical of tube coatings (cf. Calvari and Pinkerton 1999)

Table 2 Skylight and tube dimensions. Distance is from the Mauna Ulu outlet (see Online Resource 1 for locations)

Skylight	Distance (m)	Skylight width (m)	Skylight length (m)	Tube height (drained portion, m)	Roof thickness (m)
C11	160	7.7	17	1.7	3.0
SKY4	260	0.7	2.4	2.4	1.5
SKY3	320	1.5	2.4	1.4	1.0
SKY2	470	1.4	2.8	1.5	0.6
SKY1	525	1.9	2.7	0.8	1.2

backed-up behind blockages (Fig. 13b). The spiny form has the lowest vesicularties (41–54%) of all lava facies, although the mean vesicularity is still relatively high at 46 ± 6% (Table 3).

Transitional lava is characterized by rough pāhoehoe containing coiled strips of lava (cf. Peck 1966) and nascent ʻaʻā clinkers rooted in the pāhoehoe (Fig. 12f). Transitional lava has a vesicularity (mean of 52 ± 4%) between that of smooth and spiney pāhoehoe (Table 3). Finally, slabby pāhoehoe consists of broken slabs of smooth, rough or spiney pāhoehoe, as well as transitional lava, and is usually found towards flow fronts (Fig. 13c,d). Being dominated by broken slabs of smooth pāhoehoe (Fig. 13c), it has a vesicularity nearly identical to that of its parental facies; slabby and smooth pāhoehoe having mean vesicularities of 58 ± 4% and 59 ± 6%, respectively (Table 3).

ʻA ʻā is of two types: mature and immature, each distinguished by clast size and form. Mature ʻaʻā characterizes the

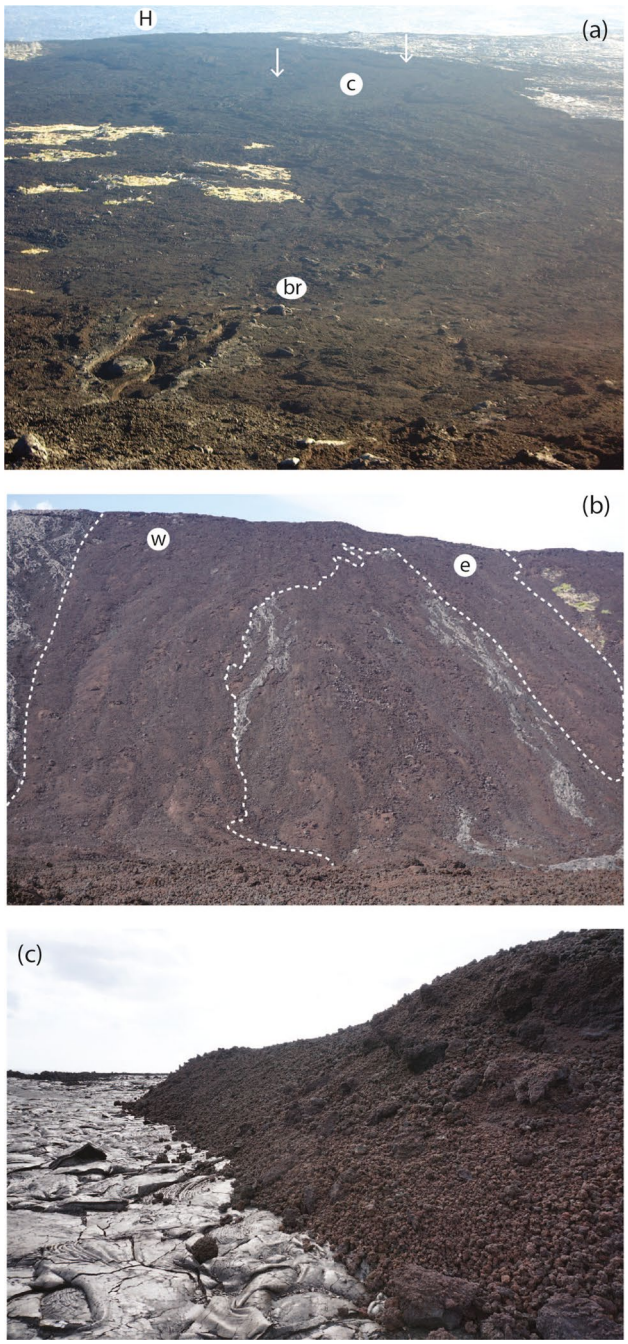

Fig. 8 Photos of the distal (transitional channel and dispersed flow) section of the channel system. **a** Viewing south from the crest of Poliokeawe Pali showing the zone of transitional channel between the end of the braided stable channel section (br) and the crest of Hōlei Pali (H). The central stream is marked "c", and broad, incipient, initial levees are marked with arrows. Distance between "br" and "H" is 2.2 km. **b** West (W) and east (e) branches of dispersed flow on Holei Pali; Pali is 110 m high. **c** 'a'ā flow front of the west branch; flow front is 3.5 ± 0.2 m high

basal unit and is composed of rounded 'a'ā clasts, often oxidized and typically 10–15 cm across. These are mixed with lava balls and rafts of pāhoehoe (Fig. 12a). Immature 'a'ā

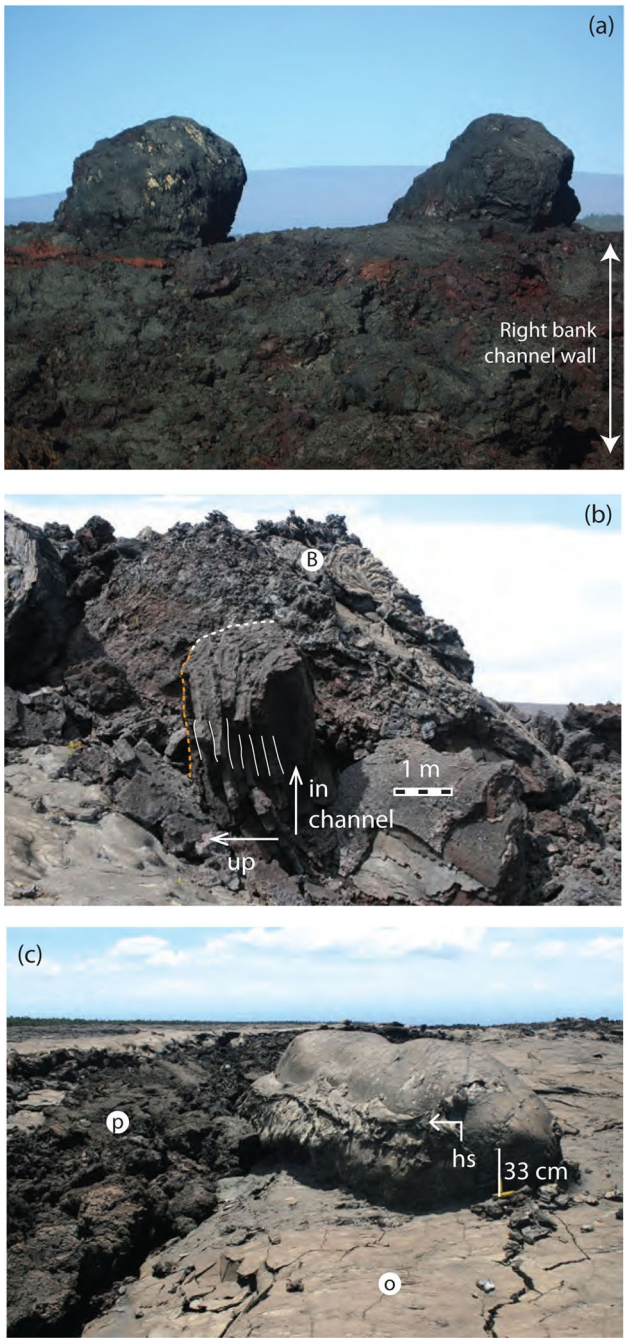

Fig. 9 Examples of lava boats. **a** Two 2-m-high lava boats coated in rough surfaced pāhoehoe overflow perched on the channel rim at COC. **b** Broken lava boat in blockage at C8 (B). Upper surface of the block is given by dashed line, where white is the channel wall section of the block, and orange is the levee surface, so that the in-situ orientation of the block before failure would have been as marked. Thin white lines mark the overflow unit contacts. **c** Lava boat (6×2 m) veneered in smooth surfaced pāhoehoe overflow lava 190 m downchannel from station C8. Channel is brim-full with ponded spiney pāhoehoe (p), and levee surface is of smooth pāhoehoe overflow (o); which also mantles the boat and is plastered to its base as a high stand marker (hs)

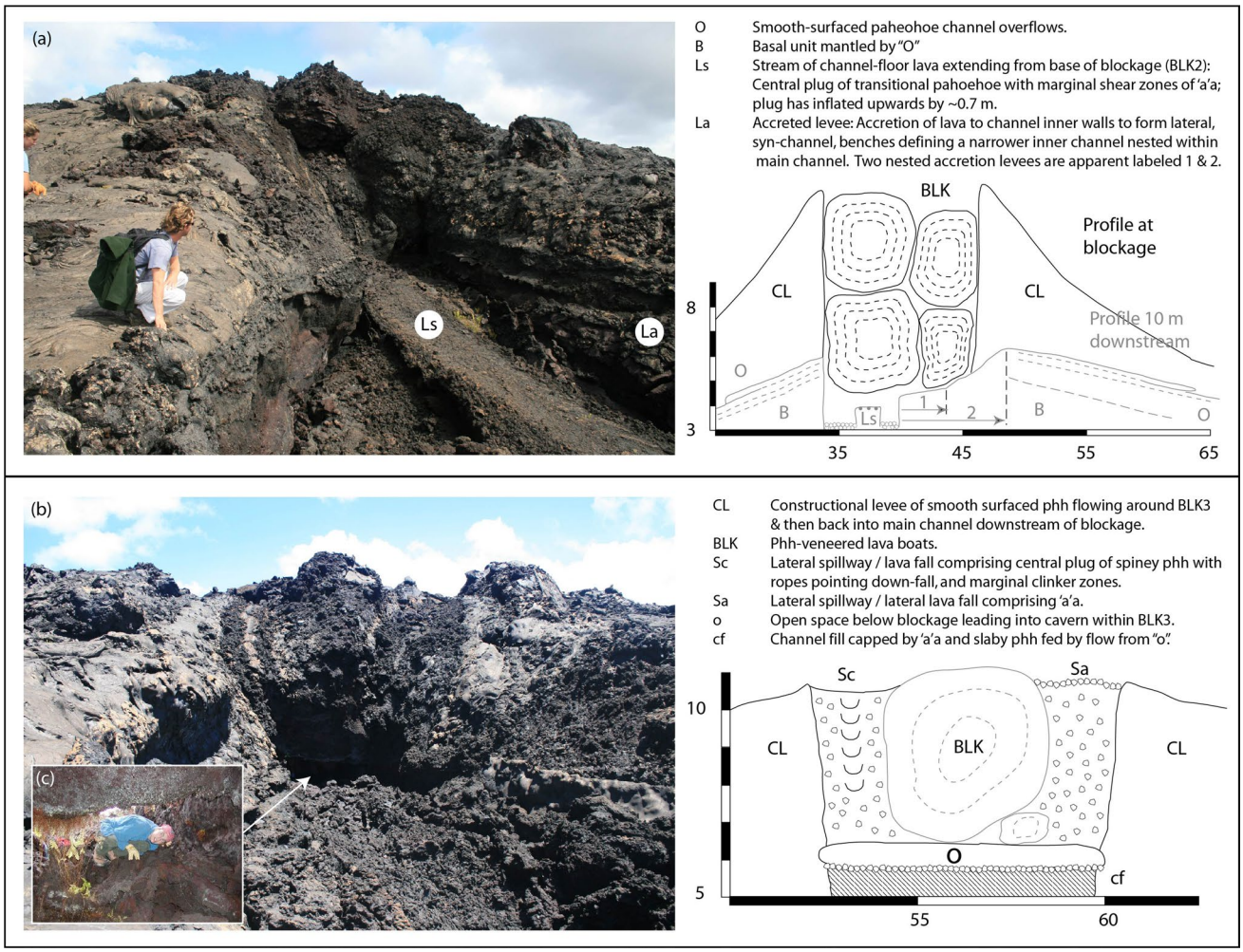

Fig. 10 Structure of channel blockages at **a** BLK2 and **b** BLK3. **c** View of a person entering the opening into the internal cavern [marked "O" on **b**] of blockage BLK3

is spiney, black-glassy, with clasts typically 3–6 cm across (Fig. 12b). It lacks lava balls and is associated with channel overflows (as in Fig. 12d) and undrained (non-ponded) channel lava (as in Fig. 11d). Where sampled at the flow front, squeeze-outs of the 'a'ā interior had vesicularities of 27–41% (Table 3).

Levee units

We can identify four unit types in the levee stratigraphy (see legend to map of Online Resource 1). These are, from the base up: basal, surge-fed overflow, blockage-fed overflow and channel breakouts.

The basal unit is typically 3 m thick (Table 4) and is made up of mature 'a'ā (Fig. 12a). It represents the stalled margin of the initial 'a'ā flow emplaced at the onset of the eruptive episode. Following Sparks et al. (1976), it therefore represents an initial levee. It crops out discontinuously in the proximal reach of the system where it is, generally, completely covered by pāhoehoe units from subsequent channel overflows (Figs. 3a and 13c). However, its line can sometimes be traced as a low pāhoehoe-mantled scarp (Figs. 4a and 13c). It crops out near-continuously between BLK 2 (Fig. 3b) and COC (Fig. 4a), but then again becomes largely buried by overflow units in the lower reach of the stable channel (Fig. 4b). The case type location for the basal unit is thus between BLK2 and COC (Fig. 13e) where the unit is 4–6 m high and ~ 130 m wide (from Online Resource 2). This is the flow within which the channel then formed.

Surge-fed overflow units are thin, typically being 18 ± 13 cm thick (based on measurements on 128 locations; Table 4). They are made up of smooth pāhoehoe in the proximal-medial reach of the channel (Fig. 13a), and of immature 'a'ā (Fig. 12b), rough pāhoehoe (Fig. 12d) and transitional (Fig. 12f) in the distal reach. Surge-fed overflow units mantle the basal unit and so were emplaced after, and onto, the

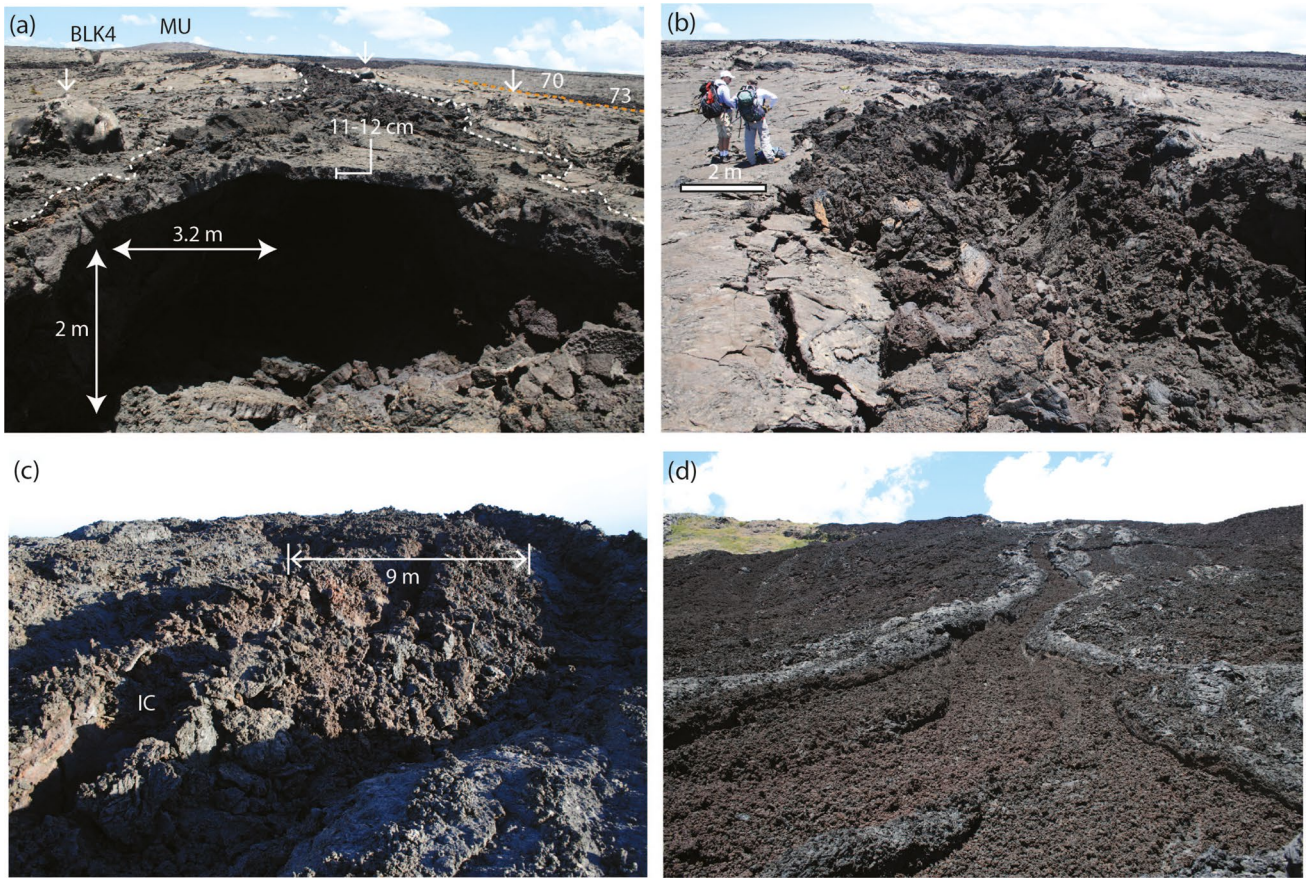

Fig. 11 Examples of syn-channel lava structures. **a** Hanging roof on drained pond of backed-up, spiney pāhoehoe. Location is 95 m up-channel of C7, and 240 m up-channel from the causative blockage. Note that levees are of smooth surfaced surge-fed overflow pāhoehoe with stranded lava boats (marked with arrows). Channel is brim-full with ponded spiney pāhoehoe, and the contact between channel lava and levee lava is marked with the white dashed line. The contact between the left bank levee base and 1970 (70) pāhoehoe and 1973 ʻaʻā (73) is marked with an orange dashed line. Channel over-construction around and upstream of blockage BLK4 and the Maun Ulu shield (MU) are apparent in the background, and rubble of blocks of spiney pāhoehoe from roof collapse are apparent in the foreground. **b** Subsided pond roof 110 m up-channel from pond-example given in (a). **c** Down-channel elongated tumulus in a syn-channel pond of transitional pāhoehoe at C13, with an inflation cleft (IC) running down the tumulus long-axis (cf. Walker 1991). **d** Undrained immature ʻaʻā in the channel on Poliokeawe Pali. Channel is 15 m wide at point of photograph, and 3–5 m wide on the Pali

initial levee during short-lived lava surges that overwhelmed the channel capacity. High stand marks on lava boats (Fig. 9c), as well as the scale of lava boats buried by overflow units (Fig. 13a), suggest that overflows involved flow 40–50 cm above bank. Orientations of stretched vesicles indicate flow back into the channel at the end of the overflow event for lava within 1–5 m of the channel (Fig. 13a). In the proximal reach where the levee slope (7–16°) is greater than the regional slope (2.8–3.5°; cf. Table 1 and Online Resource 2) overflow units flowed laterally away from the channel as extensive pāhoehoe sheet flows (Fig. 3a). Only at the base of the levee did the overflows turn to flow parallel to the channel, a direction which follows the regional slope (Fig. 13c). However, in the distal reach the levee slope (5–8°) is around that of the regional slope (5–7°; cf. Tables 1 and Online Resource 2). Here overflow units flowed down the levee in a direction parallel to the channel (Fig. 4b). In both cases, surge-fed overflow units generally entirely cover all preceding units (Figs. 3a, 4b, and 13c). Typically, two or three sheets can be mapped on the levee surface, but in cracks in the levee bank and in levee blocks comprising lava boats up to seven units can be counted (Fig. 9b). In effect, later overflows buried earlier overflows, where buried overflows are often apparent from breaks in slope in the smooth pāhoehoe cover (Fig. 13a). Surge-fed overflow units added an extra 3–4 m to the levee height, to give a typical levee total thickness at the channel rim of ~ 6 m (Table 4).

Blockage-fed overflow units are thicker than surge-fed overflow units, being 70 ± 50 cm thick (Table 4). They typically extend just a few meters (< 20 m) from the channel (Figs. 3 and 4) and are always made up of slabby and/or spiney pāhoehoe (Fig. 13b). Blockage-fed overflow units

Fig. 12 Lava facies characterizing the Muliwai a Pele channel system. **a** Mature and **b** immature ʻaʻā making up the basal unit of the right bank levee of the channel system at C13. Lava balls are marked "B". **b** Smooth surfaced pāhoehoe at station C8. **d** Rough surfaced, **e** spiney and **f** transitional pāhoehoe at C13. Canon lens cap used for scale is 6 cm across

mantle the surge-fed units, and so were emplaced after, and onto, the surge-fed overflow and initial levees during back-up and overflow due to ponding behind blockages. Blockage-fed overflows always comprise a single levee-capping unit (Fig. 13b), indicating that they were the final event in the levee construction sequence and that there was only one overflow event at this point in time. They represent ooze-over of outgassed lava that has backed-up behind blockages, as seen in the distribution of such units in relation to blockages in the proximal reach of the channel system (Fig. 3a).

Channel breakouts are secondary ʻaʻā flows fed by sustained overflow from the master channel or levee failure. The main breakout fed by sustained overflow is from behind blockage BLK2b (see map of Online Resource 1) and is mapped in detail in Fig. 3b. Here ponded lava has overflowed both the right and left banks along a channel length

of 110 m. The right bank flow is of ʻaʻā. This flowed down the levee slope before turning at the base of the levee to follow the regional slope parallel with the main channel. The unit extended 260 m, attained a width of 30–40 m and developed a 10-m-wide channel of its own flanked by simple, rubble levees. The left bank flow is of slabby pāhoehoe and, likewise, flowed laterally out of the channel and down the levee before turning south to flow parallel to the levee base. The unit extended 280 m, attained a width of 20–45 m and no channel is apparent. Together these two (left and right bank) breakout units added 50–85 m to the levee width, increasing the system width at stations C3 and C4 over the width at other locations (Fig. 6).

There is one breakout unit emplaced by levee failure. This was fed by a failure of the left bank levee behind BLK6 (see map of Online Resource 1) and is mapped in detail in Fig. 4b. The flow is ʻaʻā and contains numerous lava boats made up of lava-veneered chunks of the failed levee (Fig. 4b). Flowing parallel to the main channel, partially on and partially off of the pre-existing levee (Fig. 4b), it extended about 200 m and added 40 m to the width of the system at station C13 (Fig. 6).

Levee and channel geometry

Total unit and levee widths, i.e., the entire flow unit width, increase systematically down channel (Fig. 14a), where the total flow width increases from 50–100 m at the first station (C5) to 110–160 m at the most distal stations (C12 and C14). This is mostly due to an increase in levee width, where the right levee increases in width from 9–41 m at C8 (1.6–1.9 km down channel) to 84–96 m at C13 and C14 (4.8–5.0 km down channel). Likewise, the left levee width increases from 26 m at C7 (2.6 km down channel) to 56 m at C14 (Table 5).

Channel width data can be divided into three main segments (Fig. 14b). As far as station COC (4.4 km down channel) widths are relatively constant, having a mean and standard deviation of 9 and 3 m respectively. However, between COC and station C16 (5.1 km down channel) widths are greater (Table 5) and more variable with a mean and standard deviation of 16 and 5 m respectively. Thereafter, the channel is narrower again, being just 2–5 m (average of 3.8 m) wide between station C18 (5.3 km down channel) and the end of the channel at 5.5 km (Fig. 14b). The same three divisions can be made in terms of channel depth (Fig. 14c). As far down-flow as station COC depths are relatively constant, having a mean and standard deviation of 5.3 and 2.0 m. However, between COC and station C16 depths are greater, being up to 18.5 m, and more variable with a mean and standard deviation of 8.5 and 4.3 m (Table 5). Thereafter, between station C18 and the end of the channel depths, are 0.7–3.3 m with an average of 1.8 m (Fig. 14c).

The three-fold division in channel width and depth are reflected in the channel morphologies, where the channel can be divided into three types based on form: mature, ponded, and anabraching-braided. The mature channel form is characteristic of the distal-to-medial reach from the point of first exposure (at station C8) through COC to station C12 (at a down-flow distance of 4.5 km). The mature form is characterized by a single, well-defined channel bounded by initial rubble levees capped by surge-fed overflow levees of pāhoehoe (Fig. 15a,b). The ponded channel form begins at BLK6 (after 4.6 km, Table 1). The ponded-form can be traced to C17 (at 5.2 km). Station C17 is located at the crest of Poliokeawe Pali and at this station channel form abruptly changes to braided on the steep slopes of the Pali (Table 1). In fact, all changes in channel form are abrupt and coincide with breaks in slope, an association that is also apparent in the aerial photographs acquired during emplacement (Fig. 2).

There are three ponds down the ponded channel reach (Fig. 4b). The ponds are up to 30 m wide and 110 m long, and linked by channel sections that are much deeper than they are wide (Fig. 15c). Levees in this reach are more complex than those of the mature reach, comprising overbank flow of surge-fed transitional lava, as well as accreted levees involving layers of transitional lava plastered to the channel walls (Fig. 15c,d). Surge-fed overflows are also of immature ʻaʻā which have formed flows (often with channels) that moved parallel to the main channel (Fig. 4b). Undrained lava in ponds is inflated transitional lava and spiney pāhoehoe (Fig. 15e), whereas it is of ʻaʻā and broken slabs of transitional lava in the pond-linking channel sections (Fig. 15d). This channel form, which widens and narrows, can be seen in the aerial photograph taken on the morning of 1 June 1974 (Fig. 2a).

The distal channel reach is braided with three anabranches: east, central and west (Fig. 15f). Of these the central branch comprises the primary master channel that provided the main feed to the zone of dispersed flow (Fig. 1a). The east and west anabranches fed units that extended around 500 and 950 m down the left and right bank margins of the flow field, respectively. The east anabranch is a 20-m-wide ʻaʻā unit with an incipient channel which forms the left bank of the channel system down Poliokeawe Pali, and has its source in the third and final pond of the ponded reach (Fig. 4b). The west anabranch is a 7-m-wide channel which feeds multiple ʻaʻā flows that form the right bank of the channel. Its source is the exit of a 25-m-long tube that extends SSW through the right bank levee of the central channel. The entrance to the tube is a 2.2-m-high and 1.3-m-wide tunnel extending from the base of the right bank channel wall at the crest of Poliokeawe Pali (Fig. 15f). The air photo taken on the morning of 1 June 1974 (Fig. 2) shows the west branch to be active at the same time as the central branch. The east branch developed later in the day following breakout from the left-bank wall of pond 3 (Fig. 4b), but overlapping relationships show that all three branches would

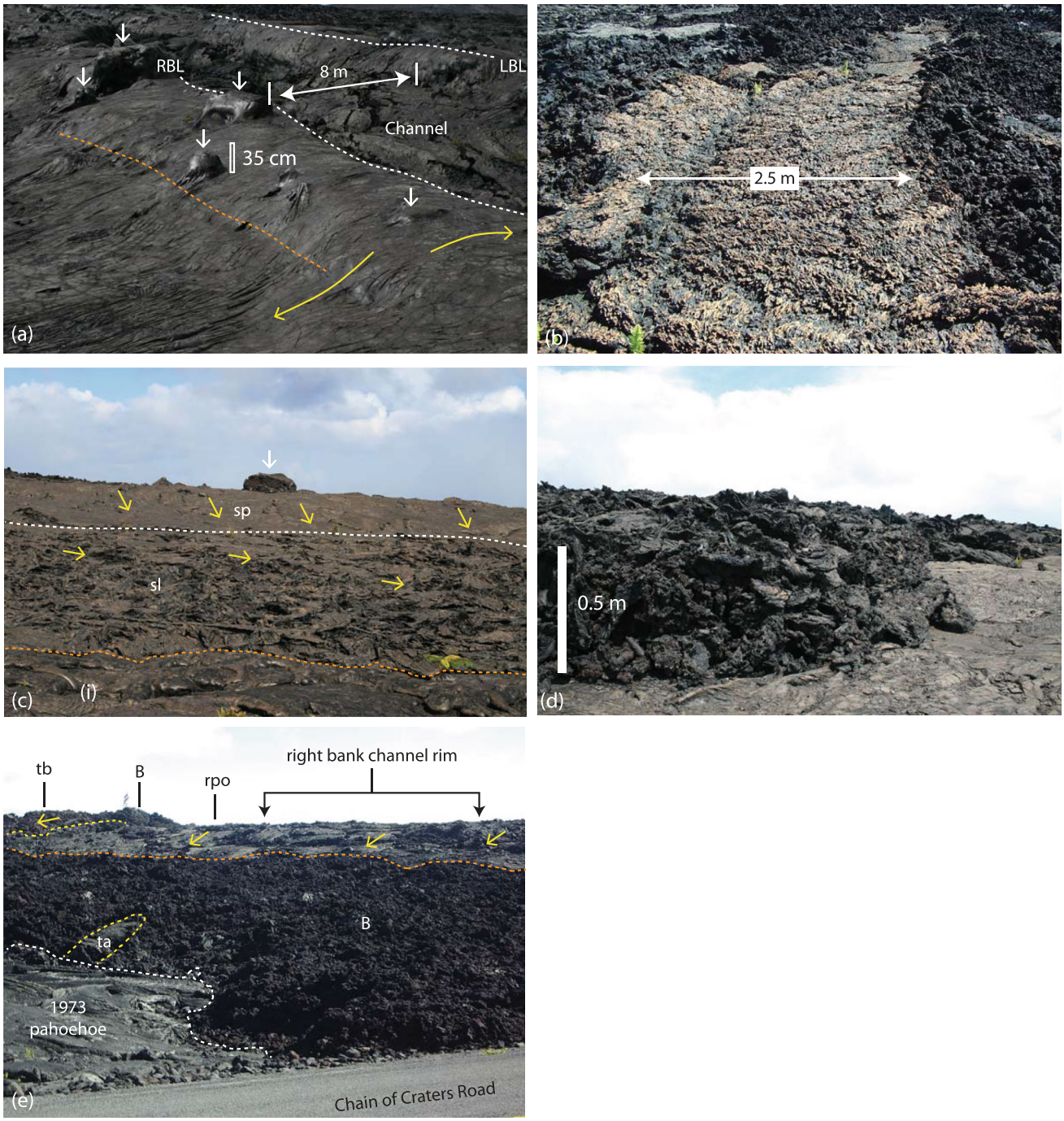

have been active at the same time (Fig. 15g). Cross-cutting relationships show that in a final stage of formation, the west anabranch cut the central channel through down-cutting by thermomechanical erosion of the west branch at the crest of the Pali. The base of the channel at the point of down-cutting is 2 m lower than the base of the central channel on the Pali (channel *c* of Fig. 15f). This cut supply to the master channel, instead feeding a short (25-m-long) flow of late-stage ʻaʻā into the upper west anabranch channel (unit *ls* of Fig. 15f).

On the steep (20°) upper slopes of Poliokeawe Pali, the central branch is a well-formed channel (Fig. 16a– d). Overbank flow forms shallower lateral channels, some with superelevation and overbank spatter, that run in and out of the main channel (Fig. 15f). At the base of Poliokeawe Pali and on more gradual (15°) slopes, the central branch becomes braided dividing into two or three branches with the channel dividing and uniting around a series of islands (Fig. 16e–f). This occurs over a short distance (100 m) before the channel

◂**Fig. 13** Levee units characterizing the Muliwai a Pele channel system. **a** Smooth surfaced pāhoehoe sheet flow between stations C8 and C8b. Lava boats stranded on the levee surface are marked with white arrows, dashed line traces the crest of the right bank (RBL) and left bank (LBL) levees, and vertical line is placed at their base (n.b. line is placed in-channel). Yellow arrows mark flow directions apparent from flow fabric, and orange dashed line marks limit of buried overflow. **b** Lateral overflow of toothpaste lava from blockage at C2 onto levee bank. Blockage overflow consists of a central plug of spiney pāhoehoe and shear zones of immature ʻaʻā. **c** Surge-fed overflow unit at station BLK4. Overflows are smooth surfaced pāhoehoe (sp) proximally, breaking up to slabby pāhoehoe (sl) distally. Contact with underlying lava (1974 pāhoehoe) is marked with dashed orange line. Note that the basal ʻaʻā unit is completely buried, but its presence is apparent from a break in slope in the levee construct (dashed white line). Channel rim is along the skyline, with stranded lava boat marked with white arrow; yellow arrows mark flow directions apparent from flow fabrics. Distance to channel rim is 30 m, and distance to the break in slope is 20 m. **d** Overbank slabby pāhoehoe from blockage overflow behind BLK4 overlying levee units of surge-fed smooth-surface pāhoehoe. **e** Basal ʻaʻā unit (B) north of the Chain of Craters road, capped by rough pāhoehoe surge overflow units (rpo) and a blockage fed overflow of spiney pāhoehoe (toothpaste, tb) from behind blockage "B". There is also a toothpaste ooze out of the interior of the flow at the base of the levee (ta). Distance from channel rim to the edge of basal unit is 45–50 m, and overflow units extend 12–20 m from the channel

system enters the zone of transitional channel and dispersed flow over slopes of 4° (Fig. 15g).

Channels on Poliokeawe Pali involve overflow levees of transitional lava, as well as nested and wall-accreted levees of immature ʻaʻā (Fig. 16). Immature ʻaʻā also comprise the undrained lava remaining on the channel floor (Figs. 11d and 15g). The channel is cut by 80–90-cm-wide cracks that opened during the November 1975 earthquake (M_S 7.1, Ando 1979; Fig. 15f) and at these locations between two and four undrained units with a total thickness of up to 3 m can be counted (Fig. 16c).

Unlike at stations in the proximal–medial channel reach, distally the channel is set down into the surrounding lava and shows much more complex levee forms (cf. Figures 6 and 16). The complexity of the distal segment of the stable channel also makes the outer-limit of the master channel levees impossible to define, as they are always buried by subsequent flow fed by ʻaʻā overflow from higher in the channel (cf. Lipman and Banks 1987). This burial process also explains why the channel is set down into the surrounding flow field (Fig. 16).

Down-channel vesicularity, crystallinity, and temperature

Vesicularity for surge-fed overflow units shows a general decrease with distance, but with a large degree of scatter (Fig. 17a), where proximal vesicularities are $65 \pm 5\%$ and distally values are $51 \pm 4\%$ (Robert et al. 2014). Phenocryst contents for the bubble-free mixture are on average $12 \pm 3\%$, and are a little higher above 3.5 km than below (Fig. 17b), declining from 13–16% proximally to 9–10% distally. The new samples obtained in 2016 allows us to fill a gap in the down-flow microlite content data given in Robert et al. (2014). Results show that microlite content for surge-fed overflows experience a down-channel increase from 3 to 16%, giving a crystallization rate (per unit distance) of approximately 0.043 Φc/km, although the rate of increase is best fit with a power law (Fig. 17b). This rate of increase contrasts with that previously determined in Robert et al. (2014), i.e., 0.03 Φc/km at the proximal reach and 0.14 Φc/km after the transitional zone. Here we note that the samples associated with overflow of lava from ponds show a higher rate of 0.11 Φc/km (Fig. 17b).

The eruption temperature of 1164 ± 2 °C, calculated from the MgO content of MU1 glass collected 1.43 km from the vent, agrees with lava temperatures of 1130 to 1165 °C measured by optical pyrometer and thermocouple in lava channels at Mauna Ulu between 1972 and 1974 (Tilling et al. 1987). In terms of cooling, the new data give cooling rates per unit distance for surge-fed overflow of 5.4 °C/km, which is less than that determined in Robert et al (2014), i.e., 6.6 °C/km. However, the ponded lava overflow samples show a higher cooling rate of 17.7 °C/km (Fig. 17c). When looking at crystallization as a function of temperature, the new data (including pond and surge samples) show two trends (Fig. A1). Between 1164 °C, where no microlites are present, and 1144 °C where microlites represent 8% of the volume, the crystallization rate is 0.003 Φc/°C. Below 1144 °C crystallization abruptly increases with a rate of 0.015 Φc/°C to 1135 °C where microlites reach 34%. This change is located between 3920 and 4365 m from the vent and corresponds to the transition from smooth pāhoehoe to transitional lava.

FLOWGO modelling

Here we update the FLOWGO modelling presented in Robert et al. (2014). This is motivated by the new sample set, the development of a new version of FLOWGO (PyFLOWGO, Chevrel et al. 2018), availability of a more precise slope profile, and additional data that we can use as a benchmark. Model initialization, as well as comparison with the benchmark, is given in Online Resource 6, where the new crystallinity and temperature data do not change the initialization conditions over those of Robert et al. (2014), but instead add further points to allow assessment of model-to-data fits.

A new slope profile was obtained for the center of the channel on a 10-m-resolution DEM and smoothed with a running mean function over 100 m (Fig. A2). As discussed in Harris (2013), application of the deterministic eight neighbors (D8) method is the basis for finding the path of steepest descent for a fluid flowing across the DEM (Mark

Table 3 Summary of pahoehoe vesicularity data of Online Resource 3

Pahoehoe facies	No. samples	Min (%)	Max (%)	Mean (%)	St. dev (%)
Smooth	44	44	74	59	6
Slabby	4	53	63	58	4
Transitional	20	44	60	52	4
Spiney	4	41	54	46	6
ʻAʻā facies	No. samples	Min (%)	Max (%)	Mean (%)	St. dev (%)
Initial levee clast	2	38	40	39	1
Interior squeeze-out	4	27	41	35	6

Table 4 Summary of levee unit thickness data of Online Resource 2 and 4. Surge-fed and blockage-fed overflow measurements are for single units, whereas the total overflow measurement is for all units

Unit	No measurements	Min (m)	Max (m)	Mean (m)	St. dev (m)
Basal	42	0.1	10	3.0	1.8
Surge-fed overflow	128	0.1	0.6	0.18	0.13
Blockage-fed overflow	23	0.1	1.65	0.67	0.45
Total levee thickness	53	1.3	18	6	3
Total overflow thickness	42	1	8	3	2

1984; O'Callaghan and Mark 1984). The D8 model assesses the gradient between a pixel and all eight of its neighbors and the flow line is projected from the host pixel in the direction of highest negative gradient. However, the D8 algorithm is well-known for having problems dealing with DEM artifacts over volcanic terrains (cf. Stevens et al. 1999), as well as long planar slopes, flat terrain, basins and pits (e.g., Fairfield and Leymarie 1991; Turcotte et al. 2001; Jones 2002). Thus smoothing of the DEM is recommended by Hutchinson (1989) to resolve these problems. Here, we find that smoothing over 100 m (equivalent to 10 pixels in this case) provides a trade-off between too much reduction in DEM detail and failure of the D8 model. Smoothing over 100 m down the channel center line produces a path of steepest descent which is identical to those obtained for the topography on either side of the channel system but, because we model flow in the channel, it is the slope of the channel centerline that we need (see Fig. 1a).

In addition, to improve the quality of the modelling, the computing step size was reduced from 200 to 10 m, as recommended by Chevrel et al. (2019). We then use the same initialization parameters as Robert et al. (2014), except that we consider the new crystallization rates as determined above (Table A1). Model output shows that the down-flow variation in temperature and crystal content can be well modelled for the surge samples, but not the ponded overflow samples (Fig. A3). The modeling also shows that the velocity of lava within the channel could have been as high as 27 m/s at the vent, decreasing to around 5 m/s at the Chain of Craters Road, but increasing again upon reaching the steep slopes of Poliokeawe (Fig. A3). These velocities served to reduce cooling rates in terms of unit distance, allowing flow to arrive at the channel exit 5.5 km from the vent with a viscosity of less than 2000 Pa s (Fig. A4), and capable of feeding flow for a further 3.5 km across the zone of transitional channel, in spite of heat losses of up to 10^8 W/m (Online Resource 6).

Discussion

The stratigraphy of the three main facies comprising the channel system (basal, surge-fed overflow, and blockage-fed overflow) shows that, temporally, the morphology of the system evolved from a simple channel between initial and rubble levees to a complex channel of compound initial, rubble, overflow and accretionary levees (Figs. 6 and 16). The resulting stratigraphy is illustrated in Fig. 15 in which first emplacement of the basal unit formed the initial and rubble levees, followed by construction of surge-fed overflow levees that buried (partially or completely) the basal unit, with accretionary levees being built during the passage of surges. Finally, ponding behind blockages capped the sequence with blockage-fed overflow levees of limited extent (cf. Harris et al. 2009).

The unconformity apparent in the south wall of Mauna Ulu is the trace of the outlet channel that fed the system (Fig. 7a). Photographs taken on 20 June 1974 show a 2-m-deep channel underlain by a ~ 5.5 m high tube (Fig. 2b). Sometime after the picture was taken, the tube roof collapsed into the tube to form the rubble-filled unconformity apparent today. Photographs taken on 1 June 1974 show a channel to be active all the way to the flow front (Fig. 2c), but the spillway out of the lake appeared to have been

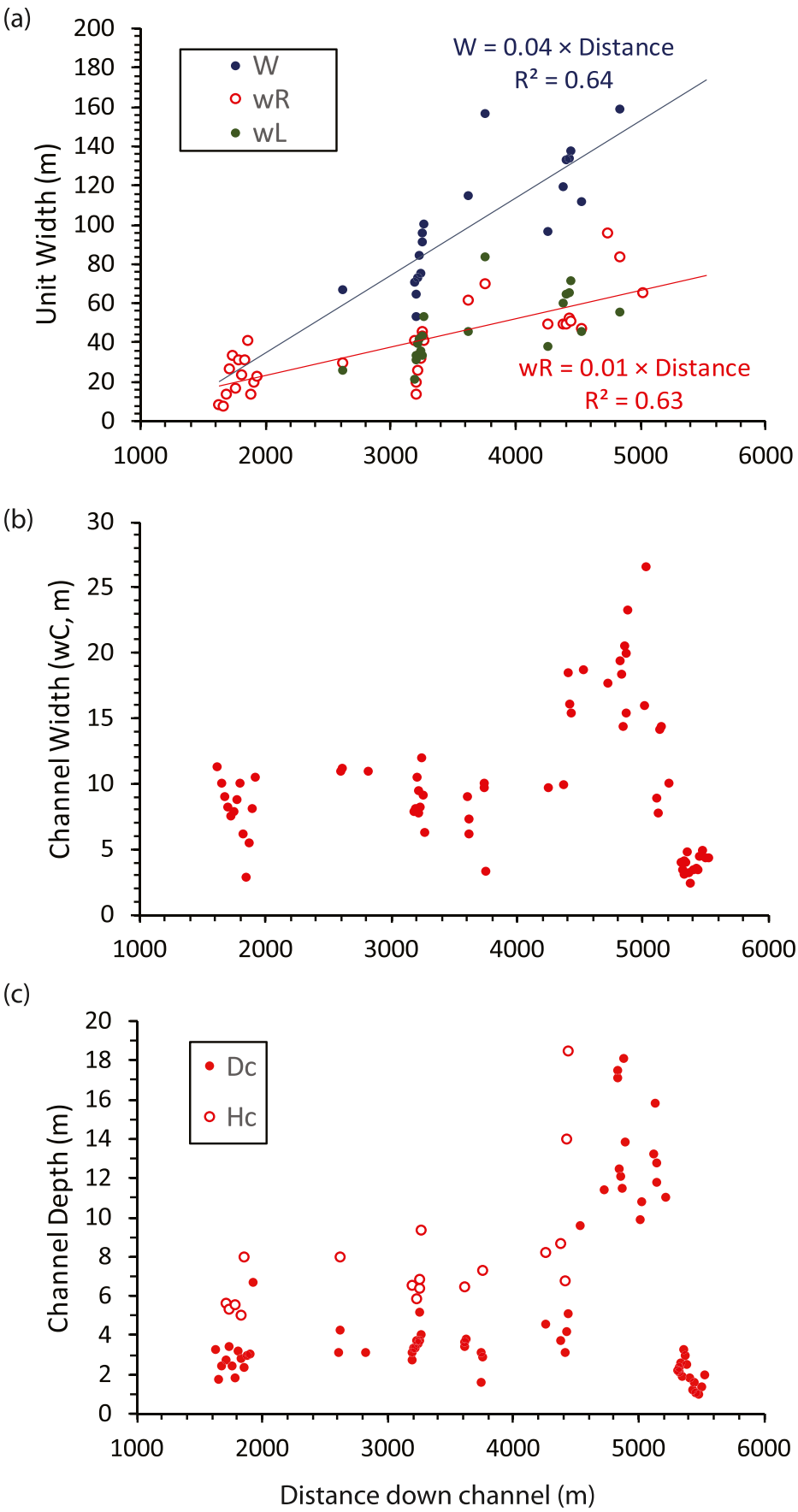

Fig. 14 Changes in **a** unit width, **b** channel width, and **c** channel depth with distance down channel. W = total unit width; wR = right bank levee width; wL = left bank levee width; Dc = Empty channel depth; Hc = total channel depth (see Fig. 5 for definitions). For each point, Dc is the median point of DL and DR at any given station, and Hc is median of HL and HR (i.e., the left and right bank values for each parameter, respectively). Data from Online Resource 2 are plotted

Table 5 Summary of levee and channel dimension data of Online Resource 2. See Fig. 5 for geometry, nomenclature and abbreviations used. Summary are for all stations where a single, mature channel can be identified, i.e., as far as the beginning of the braided channel reach at station C16. The additional width provided by channel breakout flow parallel to the main channel-levee unit is not considered

Channel/levee dimension	Above COC			Below COC		
	min	mean	max	min	mean	max
Total levee thickness (H, m)	1.3	5.3	9.4	4.9	8.5	18.5
Channel ("empty") depth (D, m)	1.1	3.0	6.7	3.3	10.9	18.1
Depth of undrained lava in channel (U, m)	0.2	2.5	6.1	2.2	7.4	13.4
Unit width (W, m)	53	93	157	112	136	159
Channel width (wC, m)	3	9	18	8	16	27
Left bank width (wL, m)	21	43	84	46	60	72
Right bank width (wR, m)	8	32	70	48	66	96

already roofed-over (Fig. 2d). Our mapping shows that the first 1.1 km of the channel system became entirely tubed (Online Resource 1) and all traces of the channel were buried by subsequent pāhoehoe from Mauna Ulu (Fig. 2d). The flow front was already at the base of the Hōlei Pali on 1 June 1974 (Fig. 2c), meaning that the channel system reached full extension in a little over 54 h, with the proximal part beginning to roof over. Thereafter, over the remaining 24 h of activity, the flow system was constructed vertically and horizontally by channel overflow, branching and breakout.

As established in Harris et al. (2009), effusion rates in the channel were highly variable with short-lived surges of bubble-rich lava overwhelming the channel capacity to emplace sheets of highly-vesicular (Table 3) and smooth-surfaced pāhoehoe (Figs. 12c and 13a). Between surges, lack of support during below bank flow caused chunks of channel wall to fail, topple into the channel, and break off to float down-channel to become lodged in constrictions and form the blockages. Blockages were porous, with decimeter-scale spaces between each boat comprising the blockage. During surges, flow thus went over as well as through the porous blockages, flowing in the gaps between the lodged boats (Fig. 10). We thus interpret the cavern and outlet system in the proximal, tubed section of the system (Fig. 7c,d) as a blockage that formed early and high up in the channel system, that later became incorporated into the tube. This structure has the same form as the interior of blockages lower in the channel (cf. Fig. 10).

With cessation of supply, lava drained down-channel to become ponded behind already-formed blockages (Harris et al. 2009). Ponds slowly filled due to down-channel drainage to overflow the channel to a limited extent (Fig. 13d; Online Resource 1). Lava also slowly seeped through the blockages to emplace late stage, channel-floor flows down channel of blockages (Figs. 10a and 11c) and to drain the ponds. Residence in the ponds caused the lava to become degassed and outgassed (Harris et al. 2009) and drainage caused unsupported pond roofs to collapse onto the channel floor (Fig. 11a,b). This explains why pond overflow units are the most dense (Table 3) and involve degassed lava forms (i.e., spiny and toothpaste pāhoehoe, Figs. 12e and 13b). The formation of blockages and stagnant ponds was a ubiquitous process that occurred 29 times down a channel length of 5.2 km, for a frequency of one blockage and pond combination every 180 m.

Down-system spatial evolution of channel morphology

We use the down-system changes in channel type, lava facies, channel-levee dimensions, and vesicularity to characterize the proximal, upper-medial, lower-medial, and distal reaches of the channel. The transitions between the four reaches are abrupt and are generally coincident with changes in substrate character and/or underlying slope.

The proximal reach extends 2.3 km from the point of first exposure to station BLK2 and is characterized by a mature channel (Fig. 15a) with extensive overflow levees of smooth pāhoehoe (Table 1, profiles C8–C5 in Fig. 6). This reach was (i) emplaced on the most gentle slopes encountered down the system (Table 6), (ii) followed the contact between two previously emplaced flow fields (Fig. 3a), and (iii) had "dense hummocky pāhoehoe produced from lava tubes" (Swanson 1973) as its substrate.

The upper-medial reach is also (i) characterized by a mature channel (Fig. 15b), (ii) was emplaced on hummocky pāhoehoe, and (iii) follows the contact between two previously emplaced flow fields (Fig. 3b). The main difference between this reach and the proximal reach is the change in the facies of the overflow levees, from smooth (Fig. 12c) to rough (Fig. 12d) pāhoehoe. This transition occurs quite abruptly between stations C3 and C2, 3.3 and 3.5 km downflow, respectively (see contact on Fig. 3b). After this point, smooth pāhoehoe is not encountered again down the system (Table 1). The levees also become wider and thicker, the channel is deeper, and overflows have a lower vesicle

content and reflect a higher yield strength than in the proximal reach (Table 6). These changes are all consistent with the rheological character of the lava crossing a threshold that pushed the lava into a transitional regime (cf. Peterson and Tilling 1980). Based on the model of Sehlke et al. (2014), this corresponds to a viscosity threshold at 200–1000 Pa s, depending on strain rate. Following Fig. 17, at 4.5 km from the source, lava flowing down this reach had a temperature of 1142–1145 °C and a microlite content of 8–13 vol.%. This is well-modelled by pyFLOWGO where, at this transition (at 4.5 km), the viscosity is modelled as being around 500 Pa s (Fig. A4), i.e., within the 200–1000 Pa s required for the change in lava character.

The lower-medial reach is characterized by a ponded channel form (Fig. 15c–e), and the levee thickness and channel depth are the greatest of any reach (cf. profiles C8–COC and C12–C16 in Fig. 6). The transition occurs abruptly between stations C12 and BLK6 (Table 1) with the first pond forming where the channel crosses onto the 1969 lava flow (see Fig. 4b). The channel down this reach is entirely on the 1969 lava flow (Fig. 4b) and is over-deepened, the channel base being 1–6 m below the surrounding pre-eruption surface at all stations (see profiles C12–C16 in Fig. 6). The 1969 lava flow is composed of fragile slabs of pāhoehoe and loose ʻaʻā clasts. Upon leaving the dense, coherent pāhoehoe surface that underlies the upper two reaches, the initial flow seems to have bulldozed into and through the 1969 lava. We suggest that this caused the flow front to stall, widen and inflate, a little like the mode of flow front advance described for ʻaʻā at Etna by Calvari and Pinkerton (1998). Upon reaching a critical pressure, lava collecting behind the stalled flow front broke out so that the flow bulldozed forward once more before stalling again. Thus, while each pond marks one of the three stalled flow front positions (Fig. 4b), the narrow, well-formed channel sections (Fig. 15c–d) mark the line of break-out flow, with the channel geometry taking on a beaded form in plan view (cf. Gorrell and Shaw 1991). Bulldozing of the underlying flow would also explain the over-deepening of this channel reach.

The distal reach has an anabranched and braided form (cf. profiles C21–C22 in Fig. 16), within which channels are narrow and shallow, but distributed across a broad (up to 300 m wide) flow field (Table 6). The aerial photograph taken of the morning of 1 June 1974 shows that at least six branches were active at the same time (Fig. 2a). This reach is 300 m long and coincides exactly with the steep slopes of Poliokeawe Pali, the reach beginning at the break-in-slope that marks the crest of the Pali, and ending at the break-in-slope that marks the Pali base (Fig. 15).

In a fluvial setting, increases in slope can lead to decreased channel depth, which cause a change to supercritical flow and avulsion associated with super-elevation (Bryant et al. 1995). This appears to have been the cause of braiding on the steepest, upper slopes of the Pali where super-elevation is apparent (Fig. 15f). The super-elevation is asymmetric, occurring on the outside of a bend (cf. Heslop et al. 1993), and caused lava to overflow out of and back into the main channel over a distance of 30 m. Other braids and anabranches are formed by overflow from the main channel typically on the outside of a curve (cf. Ferguson 1993). Overflow then moved parallel to the main channel (e.g., profile C19 of Fig. 16) rejoining it to form an anabranch, or not rejoining to from a tributary (e.g., the east branch of Fig. 15g). The morphology of the anabranch on the west side of the unit (Fig. 15f)—and its association with the fan of lava comprising the flow field on and extending from the base of Poliokeawe Pali (see map of Online Resource 1)—is reminiscent of avulsion that occurs due to sustained supply to a channel with its mouth at the head of a debris flow fan (cf. De Haas et al. 2016). Finally, braiding of the main channel at the base of Poliokeawe Pali (Fig. 15g), where slopes are reduced, is comparable to "central bar braiding" in a fluvial system (Ferguson 1993) whereby, as transport capacity declines with the reduced energy on the lower slopes, coarse material becomes deposited in the channel and is then accreted to (Ashmore 1991). Braiding requires a density difference between the deposited material and the transporting fluid (Bridge and Gabel 1992; Yang et al. 2015). In this regard, we see braiding in ʻaʻā, where the clasts have densities of up to 1910 kg/m^3, whereas the transporting fluid can have densities as low as 760 kg/m^3 (See Online Resource 3). Therefore, there is a density difference between the transporting fluid and deposited clasts by a factor of up 2.5. We thus suggest that braiding results primarily from deposition of dense ʻaʻā clasts at the base and margins of the channel under the influence of changing viscosity and flow dynamics.

Thus, the first change in channel-reach morphology (between reach 1 and 2, Table 6) is due to a rheological influence associated with lava cooling and crystallization to push viscosity, strain rate and shear stress through a threshold that causes the lava to begin to cross the pāhoehoe–ʼa ʻā transition. The second change (between reach 2 and 3, Table 6) is due to a change in substrate from consolidated to unconsolidated to initiate ponding. The final change (between reach 3 and 4, Table 6) is due to a slope increase which initiated braiding, avulsion, anabranching, and tributary formation.

Down-system vesicularity trends

Down-system there is a general decreasing trend in vesicularity (Fig. 17a), consistent with progressive down-flow outgassing, to cause an increase in density of the lava with distance (see Online Resource 3). The scatter is likely due to our sampling of overflows from a number of different surges with different source conditions where, judging from

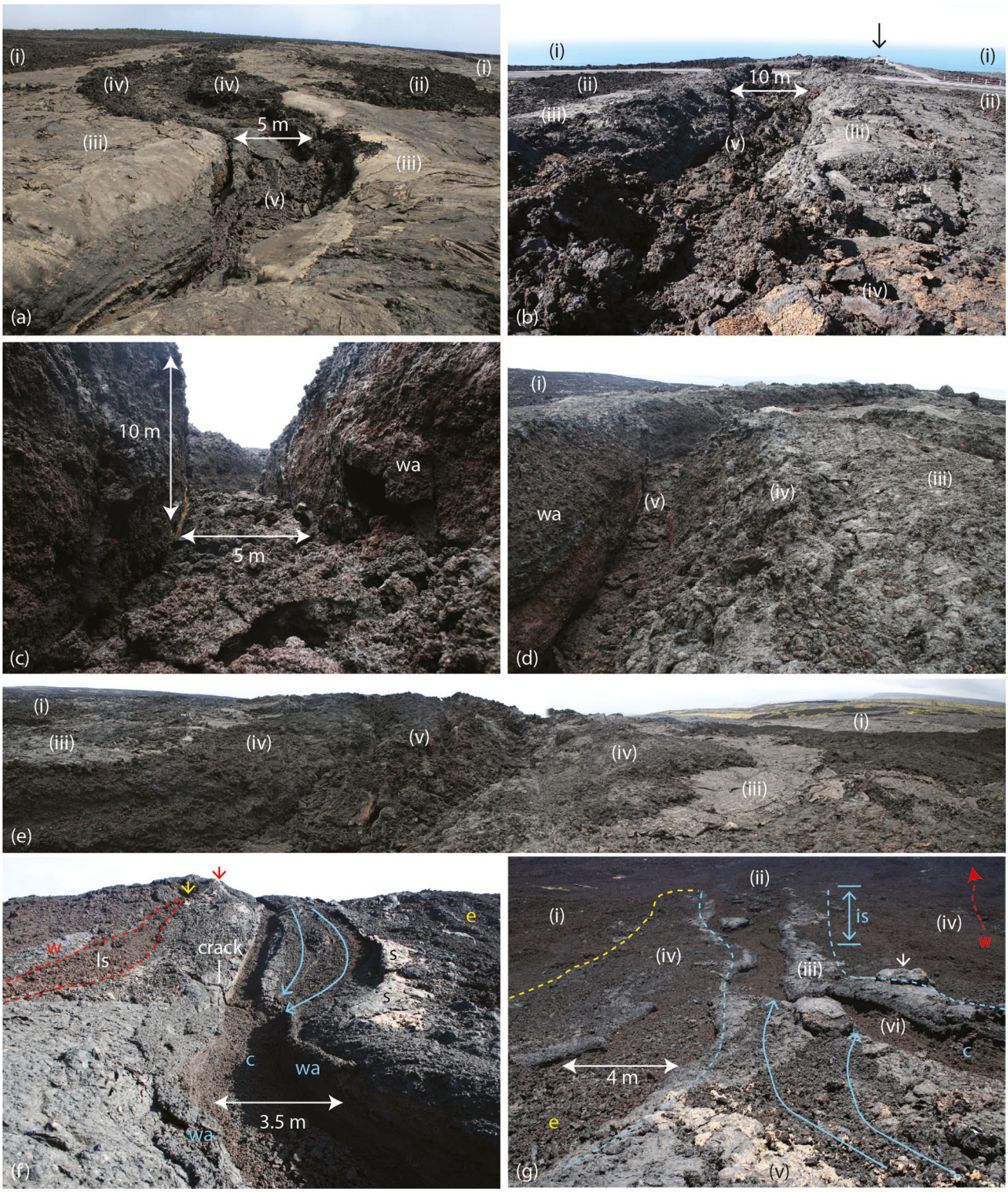

the range of vesicularities sampled within 2 km of the vent, at-vent vesicularity before outgassing could have been in the range 57–67% for any given surge. However, the trend is approximately the same for the upper and lower limits of the scatter, being around a 2% decrease in vesicularity for every kilometer travelled (Fig. 17a). Through our FLOWGO modelling (Online Resource 6), we estimate that the velocity of lava flowing in the channel between the vent and the Chain of Craters Road decreased from 27 to 5 m/s (Fig. A2), with an average velocity of 10 m/s. This compares with similar

◂**Fig. 15** **a** View down the proximal channel from blockage BLK4 (2.5 km down-channel) showing a single, well-defined, mature channel and levee stratigraphy where: units labelled (i) are the underlying flows, which are 1970 ʻaʻā (left bank) and 1974 pāhoehoe (right bank), (ii) is the basal unit, (iii) are surge-fed overflow units, (iv) are blockage-fed overflow units, and (v) is a subsided syn-channel pond roof. **b** View down the medial channel from C2 (4.3 km down-channel) towards the Mulawai o Pele overlook showing a single, well-defined, mature channel and levee stratigraphy where units are labelled as in (a) except that the underlying flows are 1969 ʻaʻā (left bank) and 1973 pāhoehoe (right bank). **c** Channel linking ponds (2) and (3) (Fig. 4b) showing channel wall accretion layers (wa). **d** Channel linking ponds (2) and (3), with legend as in (**a-c**). Note that unit (ii), the basal unit, is missing as it is completely buried (see Fig. 4b). **e** View down channel from C13 (4.7 km down-channel) into pond 2 (Fig. 4b) where units are labelled as in **a** except that the underlying flows are 1969 ʻaʻā (left bank) and 1973 pāhoehoe (right bank), and (v) is a tumulus that has formed in the pond (as enlarged in Fig. 11c). **f** Photograph looking north up the braided channel reach on Poliokeawe Pali showing the east (e), central (c), and west (w) anabranches. Red arrow gives location of tunnel from right bank central levee that feeds the west anabranch: yellow arrow gives its exit and dashed white line containing the "ls" label delimits late-stage ʻaʻā emplaced in the upper reach of this anabranch. Arrowed blue lines give direction of overflow channels that flow in and out of the master channel, and (s) denotes super-elevation with overbank spatter. **g** View down the distal channel from C18 (5.3 km down-channel) showing the central channel and levee stratigraphy where units labelled (i) are the underlying flows, which are 1969 ʻaʻā (left bank), (ii) is the main flow fed by the central braid (c), (iii) overflow levees (dashed blue lines) and island zone (is) of the central braid, (iv) are secondary flows fed by the east braid ("e": limit marked with yellow dashed line) and west braid ("w": center line marked with dashed red arrowed line); (v) super-elevated flow (blue arrows) with overbank spatter; and (vi) undrained immature ʻaʻā of central braid, i.e., the master channel

velocities measured by Lipman and Banks (1987) in the upper reach of Mauna Loa's 1984 channel-fed system, and gives a transit time of about 7 min down the first 4.5 km of the system during a surge. This converts to a bubble loss rate of around 2% per minute.

When sampled at the same locality, the vesicularity of surge-based overflow is always greater than that of overflow fed by channel-ponded lava by 2–18%, with an average difference of 8% (Online Resource 3). This is the effect of stagnant lava backing up behind blockages during late-stage channel drainage, where residence time in the ponds behind each blockage caused the pond-overflowing lava to be more outgassed when compared with the surge-fed lava. We distinguish here between degassing in the channel, where gas exolves into bubbles, and outgassing, where gas exolves into bubbles plus some bubbles are lost from the system. Here, bubble loss and thus outgassing is apparent from the lower vesicularities for the channel-ponded lava. Because near-vent lava is always of high vesicularity, bubble loss resulted from transit time down the channel and/or residence time in syn-channel ponds. The increased outgassing effect for channel-ponded lava thus results in the vesicularity of pond-fed overflows to decrease over its surge-fed counterpart, and the associated lava flow form to become that of outgassed, late-stage, facies (cf. Rowland and Walker 1987; Wilmoth and Walker 1993; Harris et al. 2017), such as spiney or toothpaste pāhoehoe (Figs. 12e and 13b). Residence time in late-stage ponds may have been as long as a few hours (Harris et al. 2009), meaning that bubble loss rates per unit time were much lower than in the surge-based case when down-system lava transit was free-flowing and fast. If we take a residence time of 4 h for late-stage pond lava (Harris et al. 2009), we have a typical loss rate of 0.03% per minute for this stagnantly outgassing case.

Levee building processes and volume partitioning

The initial basal levee was formed by lava stagnating along either side of the advancing ʻaʻā flow front (cf. Hulme 1974; Lipman and Banks 1987; Glaze et al. 2009). Given that the parental flow was ʻaʻā, the initial levee imprints the same geometry on the system as the initial flow that descended from from Mauna Ulu. This meant that a 9-m-wide channel developed between broad levees (typically 32–43 m wide) of stagnated ʻaʻā that formed in an initial flow that was 50–60 m wide (Table 5). The last point at which the basal levee can be well-defined is near the Chain of Craters road (Online Resource 1; Fig. 4b). Given the typical thickness of the basal unit (5.3 m, Table 4), this gives a total bulk volume for the basal unit down the first 4.5 km of the system of 1.8×10^6 m^3. This means that volume loss from the ʻaʻā flow contributing to initial levee construction was around 400 m^3 per meter advanced. Because widths of the initially levees increase systematically down-system (Fig. 14a), supply must have increased with time during the period of initial levee construction to allow increasing volume to be partitioned into levee construction, while ensuring continued advance. This increase would have followed the same function as given on Fig. 14a. That is, volume loss to the initial levee (as calculated from data in Online Resource 2) increased from a starting value of around 240 m^3 per meter advanced at station C8 (at 1.9 km) to 615 m^3 per meter advanced at COC (at 4.4 km), to give a rate of increase (in m^3 per meter advanced) in initial levee building capacity of 0.15 times the distance advanced (in meters).

Surge-fed overflow levees were emplaced onto the initial levees during short-lived increases in effusion rate that exceeded the channel capacity (Harris et al. 2009). Surge-fed overflow levee units are continuous as far as the Chain of Craters Road, and the average width of the left bank overflow levee is the same at stations C8 and COC, being around 20 m (as calculated from data in Online Resource 2). Given the typical thickness of each overflow unit (0.18 m, Table 4) volume loss to surge-fed overflow levee construction during each surge was thus 7.2 m^3 per meter

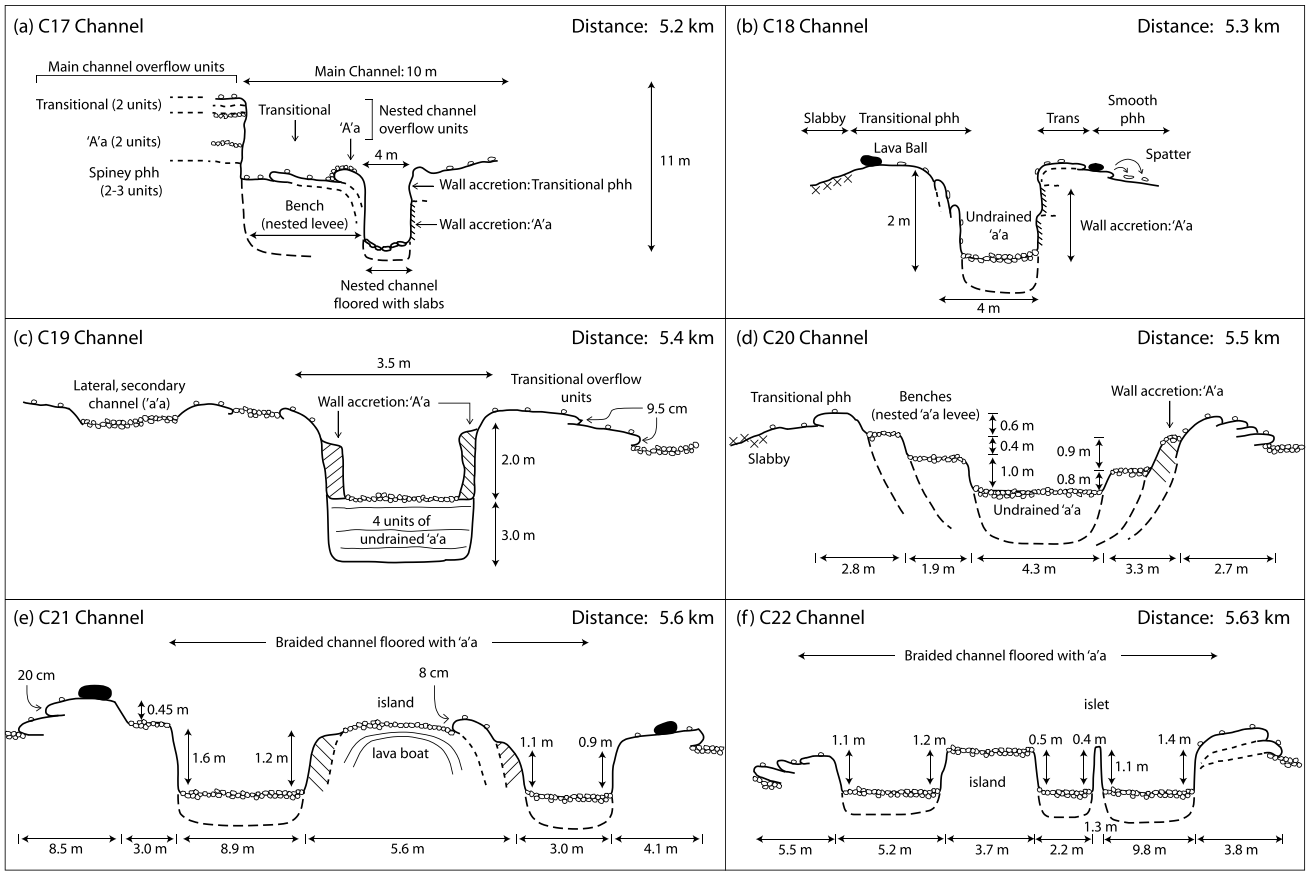

Fig. 16 Cross-channel profiles for all stations between the crest of Poliokeawe Pali (C17) and the end of the stable channel system (C22)

advanced (assuming symmetric overflow). The unvarying nature of the overflow levee width indicates that this rate of partitioning was stable down system, but would have decreased any given surge by 3.2×10^4 m^3 by the level of the Chain of Craters Road. For a typical surge at 255 m^3/s and lasting 5 min (Harris et al. 2009), this represents 42% of the surge volume, so that the surge volume would have been diminished down-channel at a rate of approximately 10% per kilometer due to partitioning of volume to the overflow levees. This down-flow volume loss meant that weaker surges became below bank with distance. These emplaced levees accreted to the channel wall or nested within the channel (e.g., Fig. 16). The surge-fed overflows contributed another 0.5×10^6 m^3 to the levees, thus accounting for 23% of the levee by volume.

Below the Chain of Craters road, surge-fed overflows are more extensive and form anabranches and tributaries (Fig. 4b). This change in channel form has two causes. First, the levee slope becomes less than that of the regional slope below the Chain of Craters road. This caused overflow to move down the levee parallel to the axis of the channel, rather than flowing laterally away from it. Second, the ponded nature of this reach appears to have caused backup in the channel due to the bottle-neck effect forced by the narrow, down-flow, pond outlet. Ponds thus served as collection points during surges, allowing sustained overflow.

Late-stage stagnant overflow levees are generally of limited extent and volume, but become more extensive down-channel (cf. Figs. 3a and 4a). This is due to late-stage flow percolating down-system through blockages so that ponds forming behind blockages higher in the system drained down-channel to incrementally sustain filling of ponds lower in the system. For the pond forming between BLK2 and C3-BLK1' this led to sustained overflow to feed two units extending several hundred meters parallel to the base of the initial levee (Fig. 3b). Instead, behind BLK6, pressure exerted on the left bank channel wall by late-stage lava ponding behind the blockage caused the bank to fail to feed a breakout of late stage lava from the pond carrying lava boats of the failed channel wall (Fig. 4b). Elsewhere, late-stage overflows added a final layer to the compound levee (Fig. 13d), and produced the final profile (Fig. 6) and mapped channel form (Online Resource 1).

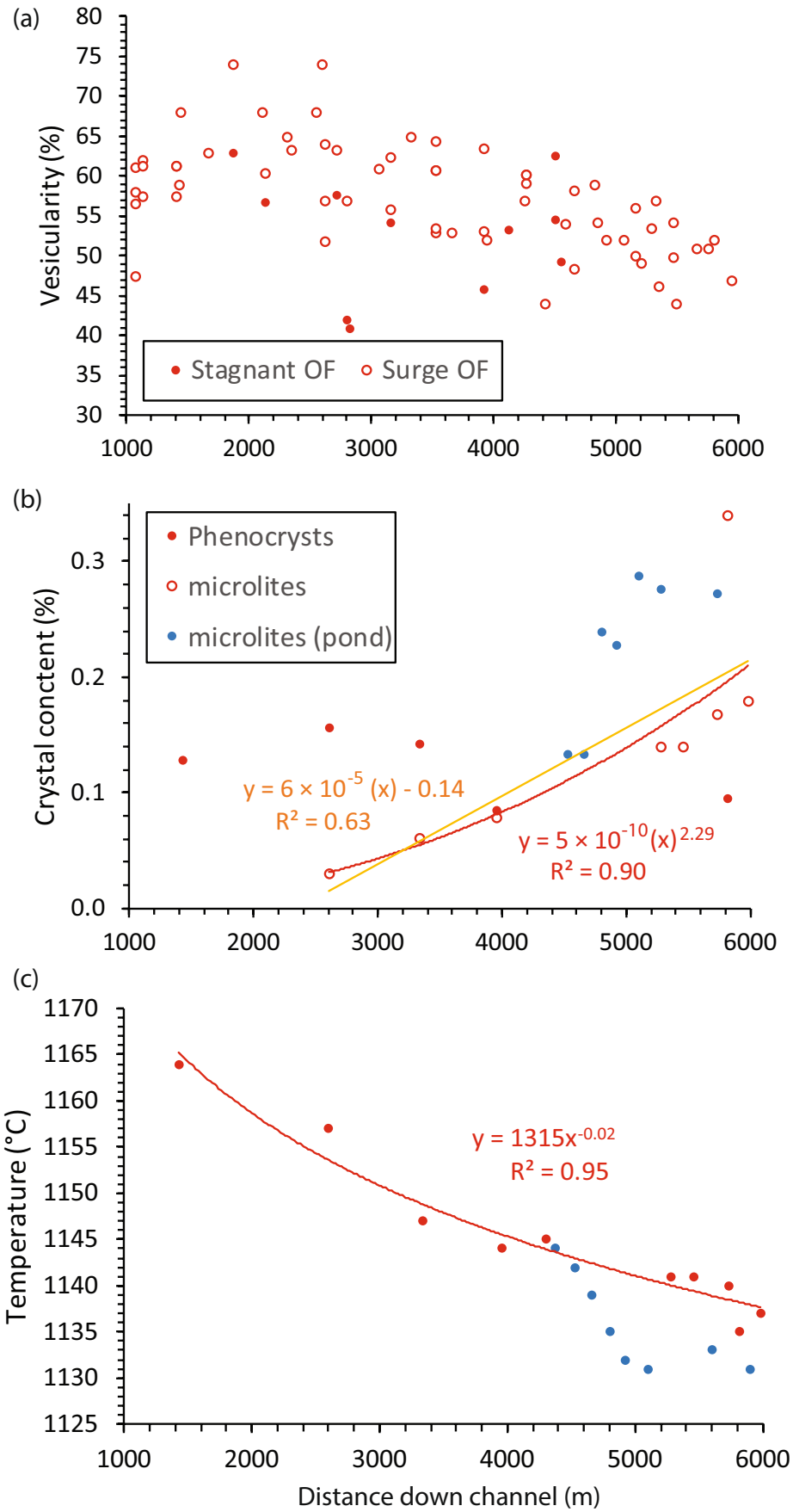

Fig. 17 Down-channel variation in **a** vesicularity (from Online Resource 3), **b** crystal content, and **c** temperature, where red- and blue-filled points are for free-flowing and channel-ponded lava, respectively (from Online Resource 5). The trends for microlites in **b** and an cooling for freely flowing lava **c** are only valid between the distances 1500 m and 6000 m, i.e., for the range of distances for which we have data. These trends thus cannot be extrapolated back to the vent or forward to the flow front. They are only valid for the channelized section. The power-law trend given in **b** is that with the best R^2 and is for microlites only. The linear fit has an $R.^2$ of 0.63, misses most points and requires a negative crystal content at 1500 m

Table 6 Lava type, dimensional and textural character of each reach. Slopes are averages for each reach from Table 1, and unit dimensions are average values taken from Online Resource 2 (with the exception of the unit width for reach 2 which is taken from the map of Online Resource 1. Vesicularity and yield strength averages are for only the surge-fed overflow units and are from Online Resource 3

Reach	Distance (km)	Channel type	Overflow levee: Lava type	Slope (°)	Unit width (m)	Unit thickness (m)	Channel width (m)	Channel depth (m)	Vesicularity (%)	Yield strength (Pa)
0	0.0 – 1.1	Tube	Buried by posterior phh	8.8	–	–	–	–	–	–
1	1.1 – 3.4	Mature	Smooth surfaced phh	3.3	80	5	9	3	62	140
2	3.4 – 4.6	Mature	Transitional phh	3.6	125	8	11	4	57	290
3	4.6 – 5.2	Ponded	Transitional phh	6.3	160	6	17	12	54	235
4	5.2 – 5.5	Braided	Immature 'a'a	16.9	250	–	4	2.5	50	410

Cooling rate and crystallization trends

Above the chain of craters road (station COC), we have clear trends in both the crystallization (Fig. 17b) and cooling rates (Fig. 17c). The cooling trend above COC of 5.4 °C km^{-1} is within the range (4–7 °C km^{-1}) found in glass chemistry samples or direct (thermocouple-based) measurements taken down other channels on Kīlauea and Mauna Loa (Crisp et al. 1994; Cashman et al. 1999; Soule et al. 2004; Riker et al. 2009; Chevrel et al. 2019). Below COC we can project the 5.4 °C km^{-1} cooling trend through the data, but a second trend of 17.7 °C km^{-1} is apparent (Fig. 17c). The same applies to the crystallization rates (Fig. 17b). We suggest that this reflects two modes of flow through the ponded reach. The first mode is free-flowing where the lava moves freely through each pond and is not held up, thereby maintaining the velocity and cooling conditions of the non-ponded channel above COC. In the second mode, lava is held up in the pond for a period of time, thus increasing the transit time of the lava down the system. This decreases the velocity of the down system passage of the lava over the free-flowing case and, thus, increases cooling and crystallization rates per unit distance. To benchmark the output of lava flow modelling only data for the free-flowing case should be used to validate model output, as in done here in Online Resource 6 (Fig. A3). The data for the ponded lava cannot be fit to output from models such as FLOWGO, as they apply to stagnant and slow cooling/crystallizing lava, such as those found in deep and stagnant lava lakes (e.g., Peck 1978; Peck et al. 1966; Wright and Okamura 1977), rather than those applicable to free-flowing lava in an unobstructed and relatively shallow lava channel.

Conclusion

The emplacement history of the Muliwai a Pele lava channel comprised three phases of emplacement (initial, free flowing and late-stage ponded) over a highly variable slope (shallow and steep) and substrate (consolidated and unconsolidated). This variety of emplacement style, slope and substrate resulted in four channel forms and geometries, five lava facies, and four levee forms. Multiplying these components together means that there are 960 possible combinations of emplacement phase, slope, substrate type, channel form, lava facies, and levee type. The varying components work together to produce a high degree of complexity to the channel geometry, lava morphology and texture, as well as cooling and crystallization rates and associated flow dynamics. All of these attributes are also highly variable in space and time, and driven by a non-constant effusion rate. This is an unacceptable degree of variance and complexity to warrant the term *stable*. Thus, we suggest that *feeder channel* is

a better term for this component of a channel-fed ‘a‘ā lava flow field. This term stresses the role of the channel in feeding dispersed flow, rather implying that the dynamics and evolution of the channel are invariable.

Although flow conditions in the feeder channel can be highly variable in both space and time, conditions for periods within the channel’s lifetime may be considered stable during a particular period if they vary only within accepted bounds within it. For example, attributes such as flow depth, width, temperature and crystallinity can be defined for periods of below-bank flow stability. During such periods, cooling trends can be physically modelled. Likewise, for periods of surge-fed overflow and late-stage ponding, trends and repeatable associations can be identified within the scatter of data apparent if all channel states (below bank, overflowing and ponded) are considered together. We demonstrate this process here and provide an interpretive guide as to how to do this as well as provide a benchmark for the below bank flow state. This state can currently be modelled using straightforward thermo-rheological relationships (Online Resource 6). However, such models now need to evolve to allow variable channel states to be taken into account and to allow the system to evolve backwards and forwards through these states as volume fluxes wax and wane.

We thus find that the construction process, and dynamics behind the construction process, of a ‘stable’ channel system to be highly unstable. That is, they are liable to change or alter (Merriam-Webster’s 2014) with distance down channel, as well as with time. The anatomy of the Muliwai a Pele channel presented here, as well as the map and data sets given in the Online Resources, present a guide to this complexity when interpreting poorly exposed, remotely sensed and/or extraterrestrial cases. We hope that these findings and datasets can also be of use in developing and framing models designed at recreating channel and levee construction conditions, for example for levee emplacement or mass partitioning to levees. Likewise, such data are needed to validate models aimed at recreating flow dynamics or thermo-rheological conditions for active lava channels feeding more distal flow zones in channel-fed ‘a‘ā lava flow systems.

Supplementary Information The online version contains supplementary material available at https://doi.org/10.1007/s00445-022-01578-0.

Acknowledgements AH warmly thanks all GG711 students who helped collect profile data and who made the data not just an immense pleasure to collect, but also made the work a magnificent learning experience for us all. For the class of 2002 this was John Bailey, Eric Bergmanis, Kate Bridges, Leon Geschwind, Christopher Gregg, Nicole Lautze, Aisha Morris, Steve Sahetapy-Engel, Murray McClintock and Steve Donegan, and in 2003, it was Matthew Patrick, Julia Sable, Patrick Shamberger and Dorsey Wanless. For the class of 2005 it was Rebecca Carey, Christopher Hamilton, Jared Marske, Melissa Rotella, Wendy Stovall and Malin Klawonn, plus the class of 2008: Andrea Steffke, Elise Rumpf, Lucas Moxley, Penny Larin, Natalie Yakos, and Tom Shea. Last, and very definitely not least, we thank Peter Jennings, who attended both the 2005 and 2008 trips, for his help, enthusiasm and humour. We are also extremely grateful to Matthew Patrick (USGS-HVO) for looking up and scanning the slides archived in the HVO library and used (with permission) in Fig. 2. We thank HVO for maintaining, and allowing researcher access to, this invaluable resource and for allowing us consult and use this precious archive. Work was carried out using the following United States Department of the Interior National Park Service (Hawaii Volcanoes NP) Scientific Research and Collecting Permits: (i) Study#: HAVO-00061, Permit#: HAVO-2001-SCI-0044, Jan 01, 2001 – Aug 16, 2005; (ii) Study#: HAVO-00141, Permit#: HAVO-2005-SCI-0049, Aug 25, 2005 – Aug 24 2006; as well as permits issued in 2012 and 2016. We are extremely grateful to HVNP for allowing us access, and as part of this permission all samples and derived data have been made openly available through the Online Resources published here. Samples are held in the depository at the Laboratoire Magmas et Volcans, Université Clermont Auvergne (Aubière, France). We thank the detailed, thoughtful and exceedingly helpful comments of two anonymous reviewers and the handling editor, Mike James, whose notes really helped focus and improve the presentation of this work. This work was funded by (i) the Hawaii Institute of Planetology and Geophysics (HIGP) and the Department of Geology and Geophysics (G&G) at the University of Manoa’s School of Oceanography and Earth Science Technology (SOEST), (ii) the Agence National de la Recherche through project ANR-LAVA (DS0902 2016; Project: ANR-16 CE39-0009), and (iii) the Laboratory of Excellence ClerVolc program 6. This is SOEST contribution number 11508, ANR-LAVA contribution number 22, and ClerVolc contribution number 547. This paper is dedicated to the memory of Peter Jennings (1941-2017).

References

Ando M (1979) The Hawaii Earthquake of November 29, 1975: Low dip angle faulting due to forceful injection of magma. J Geophys Res Solid Earth 84(B13):7616–7626. https://doi.org/10.1029/JB084iB13p07616

Applegarth LJ, Pinkerton H, James MR, Calvari S (2010) Morphological complexities and hazards during the emplacement of channel-fed `a`ā lava flow fields: A study of the 2001 lower flow field on Etna. Bull Volcanol 72:641–656. https://doi.org/10.1007/s00445-010-0351-1

Ashmore PE (1991) How do gravel-bed rivers braid? Can J Earth Sci 28:326–341

Bailey JE, Harris AJL, Dehn J, Calvari S, Rowland SK (2006) The changing morphology of an open lava channel on Mt. Etna Bull Volcanol 68:497–515

Borgia A, Linneman S, Spencer D, Morales LD, Andre JB (1983) Dynamics of lava flow fronts, Arenal Volcano, Costa Rica. J Volcanol Geotherm Res 19:303–329

Bridge JS, Gabel SL (1992) Flow and sediment dynamics in a low sinuosity, braided river: Calamus River, Nebraska Sandhills. Sedimentology 39:125–142

Bryant M, Falk P, Paola C (1995) Experimental study of avulsion frequency and rate of deposition. Geology 23:365–368

Carr MH, Greeley R (1980) Volcanic Features of Hawaii A Basis for Comparison with Mars. NASA SP-403, Washington DC, 211 pp

Calvari S, Pinkerton H (1998) Formation of lava tubes and extensive flow field during the 1991–1993 eruption of Mount Etna. J Geophys Res Solid Earth 103(Bll):27,291-27,301

Calvari S, Pinkerton H (1999) Lava Tube Morphology on Etna and Evidence for Lava Flow Emplacement Mechanisms. J Volcanol Geotherm Res 90(3–4):263–280. https://doi.org/10.1016/S0377-0273(99)00024-4

Cashman KV, ThornberKauahikaua C (1999) Cooling and crystallization of lava in open channels, and the transition of Pāhoehoe Lava to ʻAʻā. Bull Volcanol 61:306–323
Castruccio A, Contreras MA (2016) The influence of effusion rate and rheology on lava flow dynamics and morphology: A case study from the 1971 and 1988–1990 eruptions at Villarrica and Lonquimay volcanoes, Southern Andes of Chile. J Volcanol Geotherm Res 327:469–483. https://doi.org/10.1016/j.jvolgeores.2016.09.015
Chevrel MO, Labroquère J, Harris AJL, Rowland SK (2018) PyFLOWGO: an open-source platform for simulation of channelized lava thermo-rheological properties. Computers and Geosciences 111:167–180. https://doi.org/10.1016/j.cageo.2017.11.009
Chevrel MO, Harris A, Ajas A, Biren J, Gurioli L, Calabro L (2019) Investigating physical and thermal interactions between lava and trees: the case of Kīlauea's July 1974 flow. Bul Volcanol 81:6. https://doi.org/10.1007/s00445-018-1263-8
Cigolini C, Borgia A, Casertano L (1984) Intra-crater activity, aa-block lava viscosity and flow dynamics: arenal Volcano, Costa Rica. J Volcanol Geotherm Res 20:155–176. https://doi.org/10.1016/0377-0273(84)90072-6
Crisp J, Cashman KV, Bonini JA, Hougen SB, Pieri DC (1994) Crystallization history of the 1984 Mauna Loa lava flow. J Geophys Res 99:7177–7198
De Hass T, Van den Berg W, Braat L, Kleinhans MG (2016) Autogenic avulsion, channelization and backfilling dynamics of debris-flow fans. Sedimentology 63:1596–1619
Dietterich HR, Cashman KV (2014) Channel networks within lava flows: formation, evolution, and implications for flow behavior. J Geophys Res Earth Surf 119(8):1704–1724. https://doi.org/10.1002/2014JF003103
Duffield WA (1972) A naturally occurring model of global plate tectonics. J Geophys Res Solid Earth 77(14):2543–2555. https://doi.org/10.1029/JB077i014p02543
Fairfield J, Leymarie P (1991) Drainage networks from grid digital elevation models. Water Resour Res 27(5):709–717
Favalli M, Harris AJL, Fornaciai A, Pareschi MT, Mazzarini F (2010a) The distal segment of Etna's 2001 basaltic lava flow. Bull Volcanol 72:119–127. https://doi.org/10.1007/s00445-009-0300-z
Favalli M, Fornaciai A, Mazzarini F, Harris A, Neri M, Behncke B, Pareschi MT, Tarquini S, Boschi E (2010b) Evolution of an active lava flow field using a multitemporal LIDAR acquisition. J Geophys Res 115:B11203. https://doi.org/10.1029/2010JB007463
Ferguson RI (1993) Understanding braiding processes in gravel-bed rivers progress and unsolved problems. In: Best J, Bristow CS (eds) Braided Rivers, Geological Society Special Publication No. 75: 73–87
Garry WB, Zimbelman JR, Gregg TK (2007) Morphology and emplacement of a long channeled lava flow near Ascraeus Mons Volcano, Mars. J Geophys Res Planets 112(E8). https://doi.org/10.1029/2006JE002803
Glaze LS, Baloga SM, Garry WB, Fagents SA, Parcheta C (2009) A hybrid model for leveed lava flows: Implications for eruption styles on Mars. J Geophys Res 114:E07001. https://doi.org/10.1029/2008JE003278
Gorrell G, Shaw J (1991) Deposition in an esker, bead and fan complex, Lanark, Ontario, Canada. Sediment Geol 72(3–4):285–314
Greeley R (1974) Guidebook to the Hawaiian planetology conference. NASA / Ames Research Center (Moffett Field, CA): 257 p
Guest JE, Kilburn CRJ, Pinkerton H, Duncan AM (1987) The evolution of lava flow-fields: Observations of the 1981 and 1983 eruptions of Mount Etna, Sicily. Bull Volcanol 49:527–540
Harris AJL (2013) Lava Flows. Chapter 5 of Modeling Volcanic Processes: The Physics and Mathematics of Volcanism, Eds: Fagents, S., Gregg, T., and Lopes, R., Cambridge University Press, 85–106
Harris AJL, Rowland SK (2001) FLOWGO: A kinematic thermo-rheological model for lava flowing in a channel. Bull Volcanol 63:20–44. https://doi.org/10.1007/s004450000120
Harris AJL, Allen JS III (2008) One-, two- and three-phase viscosity treatments for basaltic lava flows. J Geophys Res 113:B09212. https://doi.org/10.1029/2007JB005035
Harris AJL, Flynn LP, Matias O, Rose WI, Cornejo J (2004) The evolution of an active silicic lava flow field: an ETM+ perspective. J Volcanol Geotherm Res 135:147–168
Harris AJL, Favalli M, Mazzarini F, Hamilton CW (2009) Construction dynamics of a lava channel. Bull Volcanol 71:459–474
Harris AJL, Rowland SK, Villenueve N, Thordarson T (2017) Pāhoehoe, ʻaʻā, and block lava: an illustrated history of the nomenclature. Bull Volcanol 79:7. https://doi.org/10.1007/s00445-016-1075-7
Harris A, Mannini S, Thivet S, Chevrel MO, Gurioli L, Villeneuve N, Di Muro A, Peltier A (2020) How shear helps lava to flow. Geology 48(2):154–158. https://doi.org/10.1130/G47110.1
Hazlett RW (1993) Geological Field Guide at Kilauea Volcano. Honolulu: Hawaii Natural History Association: 127 p
Hazlett RW, Hyndman DW (1996) Roadside geology of Hawai'i. Mountain Press Publishing Company (Missoula, Montana): 304 p
Helz RT, Thornber CR (1987) Geothermometry of Kilauea Iki lava lake, Hawaii. Bull Volcanol 49:651–668
Heslop SE, Wilson L, Pinkerton H, Head JW III (1993) Dynamics of a confined lava flow on Kilauea volcano, Hawaii. Bull Volcanol 51:415–432
Holcomb RT (1976) Preliminary map showing products of eruptions, 1962–1974 from the upper east rift zone of Kilauea Volcano, Hawaii. US Geol Survey Miscellaneous Studies: Map MF-811
Holcomb RT (1980) Preliminary geological map of Kilauea Volcano, Hawaii: Sheet 1 of 2. US Geol Survey Open-File Report: 80–796
Hon K, Gansecki C, Kauahikaua JP (2003) The transition from `A`a to Pāhoehoe Crust on Flows Emplaced During the Puʻu ʻŌʻō-Kūpaianaha Eruption. U.S. Geol Surv Prof Pap 1676:89–104
Hulme G (1974) The interpretation of lava flow morphology. Geophys J Roy Astron Soc 39:361–383
HVO (1974) Summary of eruptive activity. Hawaiian Volcano Observatory, US Geol Survey Monthly Report 5/21/74 – 6/20/74: 1–2
James MR, Pinkerton H, Robson S (2007) Image-based measurement of flux variation in distal regions of active lava flows. Geochem Geophys Geosyst 8:Q03006. https://doi.org/10.1029/2006GC001448
James MR, Pinkerton H, Ripepe M (2010) Imaging short period variations in lava flux. Bull Volcanol 72:671–676. https://doi.org/10.1007/s00445-010-0354-y
Jones R (2002) Algorithms for using a DEM for mapping catchment areas of stream sediment samples. Comput Geosci 28:1051–1060
Jurado-Chichay Z, Rowland SK (1995) Channel overflows of the Pohue Bay flow, Mauna Loa, Hawai'i: examples of the contrast between surface and interior lava. Bull Volcanol 57:117–126
Kerr R, Griffiths R, Cashman K (2006) Formation of channelized lava flows on an unconfined slope. J Geophys Res 111:B10206. https://doi.org/10.1029/2005JB004225
Kilburn CRJ (1981) Pāhoehoe and aa lavas: a discussion and continuation of the model of Peterson and Tilling. J Volcanol Geotherm Res 11(2–4):373–382
Kilburn CRJ, Lopes MC (1988) The growth of aa lava flow fields on Mount Etna, Sicily. J Geophys Res 93(B12):14759–14772
Kilburn CRJ, Lopes MC (1991) General patterns of flow field growth: Aa and blocky lavas. J Geophys Res 96(B12):19721–19732
Kilburn CRJ, Guest JE (1993). Aa lavas of Mount Etna, Sicily. In Active Lavas (UCL, London, UK). pp 73–106
Li Y, Liu J (2020) Late Cenozoic columnar-jointed basaltic lavas in eastern and southeastern China: morphologies, structures, and

formation mechanisms. Bull Volcanol 82:58. https://doi.org/10.1007/s00445-020-01397-1
Lipman PW, Banks NG (1987) ʻaʻā flow dynamics, Mauna Loa. US Geol Surv Prof Pap 1350:1527–1567
Mark DM (1984) Automated detection of drainage networks from digital elevation models. Cartographica 21:168–178
Marin CS, Rodriguez I, Godoy B, Gonzalez-Maurel O, Le Roux P, Medina E, Bertin D (2020) Eruptive history of La Poruña scoria cone, Central Andes, Northern Chile. Bull Volcanol: in press
Mazzarini F, Pareschi MT, Favalli M, Isola I, Tarquini S, Boschi E (2005) Morphology of basaltic lava channels during the Mt. Etna September 2004 eruption from airborne laser altimeter data. Geophys Res Lett 32:L04305. https://doi.org/10.1029/2004GL021815
Merriam-Webster's (2014) Collegiate Dictionary, 11th edition Merriam-Webster Incorporated, Springfield, p 1213
Moore HJ (1987) Preliminary estimates of the rheological properties of 1984 Mauna Loa Lava. In: U.S. Geological Survey Prof Pap 1350: 1569–1588
Moore JG, Phillips RL, Grigg RW, Peterson DW, Swanson DA (1973) Flow of Lava into the Sea, 1969–1971, Kilauea Volcano, Hawaii. GSA Bull 84(2):537–546. https://doi.org/10.1130/0016-7606(1973)84%3c537:FOLITS%3e2.0.CO;2
Naranjo JA, Sparks RSJ, Stasiuk JV, Moreno H, Ablay GJ (1992) Morphological, structural and textural variations in the 1988–1990 andesite lava of Lonquimay Volcano, Chile. Geol Mag 129(6):657–678
O'Callaghan JF, Mark DM (1984) The extraction of drainage networks from digital elevation dat. Comput Vis Graph Image Process 28:323–344
Parchetta CE, Houghton BF, Swanson DA (2012) Hawaiian fissure fountains 1: decoding deposits–-episode 1of the 1969–1974 Mauna Ulu eruption. Bull Volcanol 74:1729–1743. https://doi.org/10.1007/s00445-012-0621-1
Passey MR, Bell BR (2007) Morphologies and emplacement mechanisms of the lava flows of the Faroe Islands Basalt Group, Faroe Islands, NE Atlantic Ocean. Bull Volcanol 70:139–156. https://doi.org/10.1007/s00445-007-0125-6
Peck DL (1978) Cooling and vesiculation of Alae lava lake, Hawaii. US Geol Surv Prof Pap 935-B:1–59
Peck DL (1966) Lava coils of some recent historic flows, Hawaii. U. S. Geological Survey Professional Paper P 0550-B: B148-B151
Peck DL, Wright TL, Moore JG (1966) Crystallization of tholeiitic basalt in Alae lava lake, Hawaii. Bull Volcanol 29:487–498
Peterson DW, Holcomb RT, Tilling RI, Christiansen RL (1994) Development of lava tubes in the light of observations at Mauna Ulu, Kilauea Volcano, Hawaii. Bull Volcanol 56:343–360. https://doi.org/10.1007/BF00326461
Pukui MK, Elbert SH (1986) Hawaiian Dictionary. University of Hawaii Press (Honolulu, Hawaii): 572 p
Peterson DW, Tilling RI (1980) Transition of basaltic lava from pāhoehoe to aa, Kilauea Volcano, Hawaii: field observations and key factors. J Volcanol Geotherm Res 7(3–4):271–293
Rhéty M, Harris A, Villeneuve N, Gurioli L, Médard E, Chevrel O, Bachèlery P (2017) A comparison ofcooling-limited and volume-limited flow systems: Examples from channels in the Piton de la Fournaise April 2007 lava-flow field. Geochem Geophys Geosyst 18. https://doi.org/10.1002/2017GC006839
Riker JM, Cashman KV, Kauahikaua JP, Montierth CM (2009) The length of channelized lava flows: insight from the 1859 eruption of Mauna Loa Volcano, Hawaii. J Volcanol Geotherm Res 183:139–156
Robert B, Harris A, Gurioli L, Medard E, Sehlke A, Whittington AG (2014) Textural and rheological evolution of basalt flowing down a lava channel. Bull Volcanol 76(6):824. https://doi.org/10.1007/s00445-014-0824-8
Rowland SK, Walker GPL (1987) Toothpaste lava: characteristics and origin of a lava structural type transition between pāhoehoe and ʻaʻā. Bull Volcanol 49:631–641
Sage LL (2000) A study of dense, glassy flows: dense Pāhoehoe Lava Flows From Kilauea Volcano, Hawaii. Mcnair Scholars J 4(1):33–41
Sehlke A, Whittington A, Robert B, Harris A, Gurioli L, Médard E (2014) Pāhoehoe to `a`a transition of Hawaiian lavas: an experimental study. Bull Volcanol 76:876. https://doi.org/10.1007/s00445-014-0876-9
Soldati A, Harris AJL, Gurioli L, Villeneuve V, Rhéty M, Gomez F, Whittington A (2018) Textural, thermal, and topographic constraints on lava flow system structure: the December 2010 eruption of Piton de la Fournaise. Bull Volcanol 80:74. https://doi.org/10.1007/s00445-018-1246-9
Soule SA, Cashman KV, Kauahikaua JP (2004) Examining flow emplacement through the surface morphology of three rapidly emplaced, solidified lava flows, Kilauea Volcano, Hawaii. Bull Volcanol 66:1–14
Sparks RSJ, Pinkerton H (1978) Effect of degassing on rheology of basaltic lava. Nature 276:385–386
Sparks RSJ, Pinkerton H, Hulme G (1976) Classification and formation of lava levees on Mount Etna, Sicily. Geology 4:269–271
Suh CE, Stansfield SA, Sparks RSJ, Njome MS, Wantim MN, Ernst GGJ (2011) Morphology and structure of the 1999 lava flows at Mount Cameroon Volcano (West Africa) and their bearing on the emplacement dynamics of volume-limited flow. Geol Mag 148(1):22–34
Stevens NF, Wadge G, Murray JB (1999) Lava flow volume and morphology from digitised contour maps: a case study at Mount Etna, Sicily. Geomorphology 28:251–261
Sykes JB (1982) The Concise Oxford English Dictionary. Oxford Univ Press (New York) 7th edition: 1260 pp
Swanson DA (1973) Pāhoehoe Flows from the 1969–1971 Mauna Ulu Eruption, Kilauea Volcano, Hawaii. GSA Bull 84(2):615–626. https://doi.org/10.1130/0016-7606(1973)84%3c615:PFFTMU%3e2.0.CO;2
Swanson DA, Duffield WA, Jackson DB, Peterson DW (1979) Chronological narrative of the 1969–71 Mauna Ulu eruption of Kilauea Volcano, Hawaii. US Geol Survey Prof Pap 1056: 55 p
Tallarico A, Dragoni M (1999) Viscous Newtonian laminar flow in a rectangular channel: application to Etna lava flows. Bull Volcanol 61:40–47
The Arts Cool Graphics Group (2006) Gray scale and value finder. Color Wheel Company, Philomath (OR) 2 p
Tilling RI (1987) Fluctuations in surface height of active lava lakes during 1972–1974 Mauna Ulu Eruption, Kilauea Volcano, Hawaii. J Geophys Res Solid Earth 92(B13):13721–13730. https://doi.org/10.1029/JB092iB13p13721
Tilling RI, Christiansen RL, Duffield WA, Endo ET, Holcomb RT, Koyanagi RY, Peterson DW, Unger JD (1987) The 1972–1974 Mauna Ulu eruption, Kilauea Volcano: an example of quasi steady-state magma transfer. In: Decker RW, Wright TL, Stauffer PH (eds) Volcanism in Hawaii, volume 1. US Geol Survey Prof Pap 1350: 405–470
U.S. Geological Survey (2017) USGS US Topo 7.5-minute map for Makaopuhi Crater, HI 2017: USGS - National Geospatial Technical Operations Center (NGTOC). https://www.sciencebase.gov/catalog/item/59b39a6ee4b08b1644d81902
Walker GPL (1967) Thickness and Viscosity of Etnean Lavas. Nature 213:484–485
Walker GPL (1991) Structure, and origin by injection of lava under surface crust, of tumuli, "lava rises", "lava-rise pits", and "lava-inflation clefts" in Hawaii. Bull Volcanol 53:546–558. https://doi.org/10.1007/BF00298155

Wantim MN, Kervyn M, Del Marmol M-A, Suh CE, Jacobs P (2013) Morpho-Structure of the 1982 Lava Flow Field at Mount Cameroon Volcano, West-Central Africa. Int J Geosci 24:564–583. https://doi.org/10.4236/ijg.2013.43052

Whelley PL, Garry WB, Hamilton CW, Bleacher JE (2017) LiDAR-derived surface roughness signatures of basaltic lava types at the Muliwai a Pele Lava Channel, Mauna Ulu, Hawai'i. Bull Volcanol 79:75. https://doi.org/10.1007/s00445-017-1161-5

Whittow J (1984) Dictionary of Physical Geography. Penguin Books Harmondsworth, 591 p

Wilmoth RA, Walker GPL (1993) P-type and S-type pāhoehoe: a study of vesicle distribution patterns in Hawaiian lava flows. J Volcanol Geotherm Res 55:129–142

Wright TL, Okamura RT (1977) Cooling and crystallization of tholeiitic basalt, 1965 Makaopuhi lava lake, Hawaii. US Geol Surv Prof Pap 1004:1–7

Yang H, Lin B, Zhou J (2015) Physics-based numerical modelling of large braided rivers dominated by suspended sediment. Hydrol Process 29:1925–1941